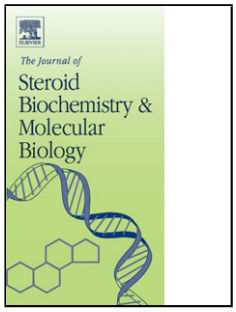

Title: Synthesis of a novel analog of calcitriol and its biological evaluation as antitumor agent

Authors: María Julia Ferronato, Diego Javier Obiol, Eliana Noelia Alonso, Josefina Alejandra Guevara, Silvina Mariela Grioli, Marilina Mascaró, Marcos Lois Rivadulla, Andrea Martínez, Generosa Gómez, Yagamare Fall, Mario Alfredo Quevedo, Alejandro Carlos Curino, María Marta Facchinetti

PII: S0960-0760(18)30161-4
DOI: https://doi.org/10.1016/j.jsbmb.2018.08.006
Reference: SBMB 5196

To appear in: *Journal of Steroid Biochemistry & Molecular Biology*

Received date: 15-3-2018
Revised date: 27-7-2018
Accepted date: 12-8-2018

Please cite this article as: Ferronato MJ, Obiol DJ, Alonso EN, Guevara JA, Grioli SM, Mascaró M, Rivadulla ML, Martínez A, Gómez G, Fall Y, Quevedo MA, Curino AC, Facchinetti MM, Synthesis of a novel analog of calcitriol and its biological evaluation as antitumor agent, *Journal of Steroid Biochemistry and Molecular Biology* (2018), https://doi.org/10.1016/j.jsbmb.2018.08.006

Synthesis of a novel analog of calcitriol and its biological evaluation as antitumor agent.

María Julia Ferronato[1⌘], Diego Javier Obiol[1⌘], Eliana Noelia Alonso[1], Josefina Alejandra Guevara[1], Silvina Mariela Grioli[1], Marilina Mascaró[1], Marcos Lois Rivadulla[2], Andrea Martínez[2], Generosa Gómez[2], Yagamare Fall[2], Mario Alfredo Quevedo[3], Alejandro Carlos Curino[1], María Marta Facchinetti[1]*.

1. Laboratorio de Biología del Cáncer, Instituto de Investigaciones Bioquímicas de Bahía Blanca (INIBIBB), Universidad Nacional del Sur (UNS) – CONICET, Departamento de Biología, Bioquímica y Farmacia (UNS), Bahía Blanca, Argentina.

2. Departamento de Química Orgánica, Facultad de Química e Instituto de Investigación Sanitaria Galicia Sur (IISGS), Universidad de Vigo, 36200, España.

3. Unidad de Investigación y Desarrollo en Tecnología Farmacéutica (UNITEFA-CONICET), Facultad de Ciencias Químicas, Ciudad Universitaria, Universidad Nacional de Córdoba, Córdoba, Argentina.

⌘ These authors contributed equally to this work.

* Corresponding author

Laboratorio de Biología del Cáncer

Instituto de Investigaciones Bioquímicas de Bahía Blanca (INIBIBB-UNS-CONICET)

Centro Científico Tecnológico Bahía Blanca

Camino La Carrindanga Km. 7 - C.C. 857

8000, Bahía Blanca, Argentina

Ph: (54) 291-4861201 ext. 130

Fax: (54) 291-4861200

E-mail address: facchinm@criba.edu.ar

GRAPHICAL ABSTRACT

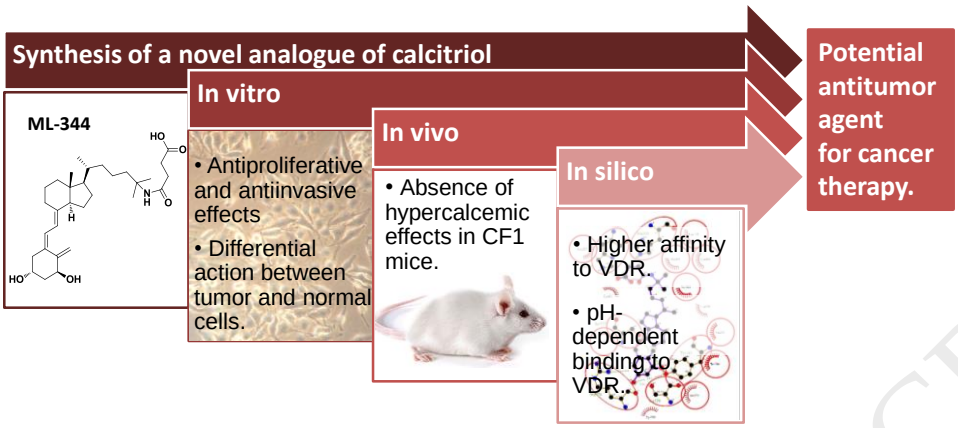

HIGHLIGHTS

- ML-344 is a novel calcitriol analogue with amide and carboxyl groups in its side chain
- ML-344 has antitumor activity in cell lines representing different cancer types
- ML-344 exerts a differential action between tumor and normal cells
- ML-344 has a differential binding to VDR between tumor and normal cells
- ML-344 does not produce hypercalcemia in mice

ABSTRACT

Calcitriol analogs have shown promising potential as compounds to be used in cancer chemotherapy. This report presents the synthesis of a novel vitamin D_3 derivative with an amide and a carboxyl group in its side chain, called

ML-344. In addition, we report its *in vitro* antitumor activity and its *in vivo* calcemic effects. We demonstrate that the analog decreases cell viability and retards cell migration of different breast, glioblastoma and head and neck cancer cell lines. Additionally, unlike calcitriol, ML-344 does not display citotoxicity to the murine non-malignant mammary cells and human astrocytes. In concordance with the antimigratory effects found in breast cancer cells, ML-344 decreased the invasive capacity and induced a rearrangement of the actin cytoskeleton in the LM3 breast cancer cell line. In relation to the *in vivo* studies, the analog did not cause hypercalcemic effects in CF1 mice administered daily at 5 µg/Kg of body weight during a period of 264 h. Finally, computational studies were performed to evaluate the potential binding of the analog to the vitamin D receptor and the *in silico* assays showed that ML-344 is able to bind to VDR with interesting particularities and greater affinity than calcitriol. Altogether, these results suggest that ML-344 has a promising potential as an antitumor agent with a differential effect between tumor and non-malignant cells.

KEYWORDS: Calcitriol; Vitamin D; Analog; Cancer; Treatment; Antitumor

1. INTRODUCTION

Vitamin D_3 is the precursor to the potent steroid hormone calcitriol (1α, 25-dihydroxyvitamin D_3) that regulates mineral homeostasis and bone metabolism [1]. In addition to this classic function, this compound has shown preventive and therapeutic properties against various hyperproliferative diseases, including cancer [2]. In this regard, calcitriol has demonstrated potent antitumor activities both in *in vitro* and *in vivo* assays in several types of cancer. However, this molecule is still not clinically used for cancer treatment because of its potential to induce hypercalcemia at the concentrations required to elicit its antitumor effects [3]. Based on these data, some strategies have been proposed to overcome this problem. On the one hand, changes have been made in the administration of calcitriol (intermittent doses) and/or its combination with other compounds, i.e. dexamethasone that increases the cytotoxic activity and mitigates calcitriol- induced hypercalcemia [4]. On the other hand, novel vitamin D analogs are being developed with the aim at finding one with low calcemic properties that

can be administered at continuous doses and that retain or even increase the calcitriol-anticancer activity.

It is known that calcitriol exerts its antitumor effects through genomic and non-genomic pathways. In both mechanisms of action the participation of the vitamin D receptor (VDR) has been described [5]. This receptor is a member of the nuclear family of receptors and it is distributed in many normal and tumor tissues [6,7]. When calcitriol binds to VDR, it heterodimerizes with the nuclear retinoid X receptor (RXR) and this complex (calcitriol-VDR-RXR) subsequently recruits cofactors to the vitamin D response elements (VDRE) in the promoter region of target genes [3,5]. Among the main groups of genes whose expression is modulated by calcitriol are those involved in calcium/phosphorous homeostasis, detoxification, immune response, cellular proliferation, differentiation, senescence, apoptosis and autophagy [2]. However, the hormone-regulated genes seem to be largely cell-type specific, based on the ratio of co-activators and co-repressors present in the cell [1,8]. Consequently, it is important to evaluate the action of calcitriol or its analogs in each tissue or cellular type.

In the present study, we report the synthesis of a novel analog of calcitriol called ML-344 bearing an amide group bonded to carbon 25 (C-25) and a carboxyl group in its side chain, and the subsequent investigation of its biological properties by means of *in vitro*, *in vivo* and *in silico* assays. To our knowledge, this is the first report that describes the synthesis and the biological evaluation of an analog with these chemical characteristics.

2. MATERIALS AND METHODS

2.1. CHEMISTRY

2.1.1. Synthetic procedures

Solvents were purified and dried by standard procedures before use. Melting points are uncorrected. ^{1}H NMR and ^{13}C NMR spectra were recorded with a Bruker ARX-400 spectrometer (400 MHz for ^{1}H NMR, 100.61 MHz for ^{13}C NMR) using TMS as internal standard (Chemical shifts in δ values, J in Hz). Flash chromatography (FC) was performed on silica gel (Merck 60, 230-400 mesh); analytical TLC was performed on plates precoated with silica gel (Merck 60 F254,

0.25mm). Mass spectra (FAB, EI) were recorded using FISONS VG and electron spray ionization (ESI-MS) spectroscopy was recorded using Bruker FTMS APEXIII. Optical rotations were obtained using a Jasco P-2000 polarimeter. IR spectra were recorded on a JASCO FT/I(R)-6100 spectrophotometer.

(1R,3S,Z)-5-{2-[(1R,3aS,7aR,E)-7a-methyl-1-((R)-6-methyl-6-nitroheptan-2-yl)octahydro-4H-inden-4-ylidene]ethylidene}-4-methylenecyclohexane-1,3-diyl)bis(oxy))bis(tert-butyldimethylsilane) (4)

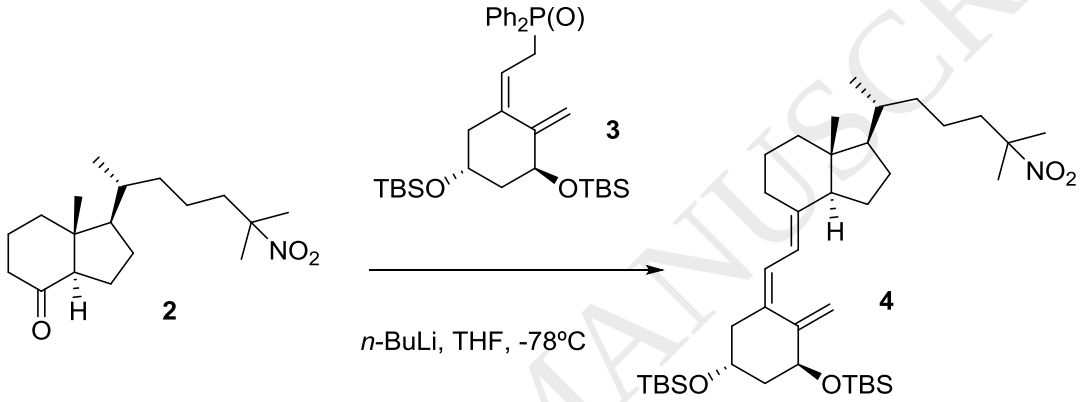

n-BuLi (216 µL, 0.54 mmol, 2.5M solution in hexanes) was added dropwise to a solution of dry phosphine oxide **3** (349 mg, 0.60 mmol) in THF (5 mL) at -78 ºC. The resulting red solution was stirred at -78 ºC for 1 h, before adding dropwise via cannula, a solution of ketone **2** (93 mg, 0.30 mmol) in THF (5 mL). Stirring was continued for 2 h at -78 ºC, in the dark. The reaction was quenched with an aqueous saturated solution of NH_4Cl (10 mL) and the mixture allowed to reach room temperature. The reaction mixture was extracted with EtOAc (3 x 5 mL) and the combined organic phases dried (Na_2SO_4), filtered and concentrated under vacuum, affording a residue which was chromatographed on silica gel using 2% EtOAc/hexane as eluent, affording compound **4** (168 mg, 83%) as a colourless liquid.

Compound **4**: Rf: 0.73 (20% EtOAc/Hexane); IR (NaCl, cm^{-1}): 2924, 2861, 1536, 1282, 1223, 1202, 1040, 986, 723,624; $[\alpha]^{23}_D$ = -12.7 (c 1, CH_3Cl).

^{1}H-NMR ($CDCl_3$, δ): 6.25 (1H, d, J = 11.1 Hz, H-6), 6.03 (1H, d, J = 11.1Hz, H-7), 5.19 (1H, br s, H-19), 4.87 (1H,br s, H-19), 4.36 (1H, m, H-1),4.19 (1H, m, H-3), 2.83 (1H, d, J = 12.1 Hz), 2.44 (1H, m), 2.23 (1H, dd, J =12.9, 7.5 Hz), 1.98

(3H, m), 1.81 (6H, m), 1.66 (2H, d, J = 13.0 Hz), 1.56 (6H, s,CH_3-26, CH_3-27), 1.44-1.13 (9H, m), 0.88 (21H, m, C-^{t}Bu-Si, CH_3-21), 0.51 (3H, s, CH_3-18), 0.08 (12H, s, CH_3-Si).

^{13}C-NMR ($CDCl_3$, *δ):* 148.3 (C-10), 140.9 *(*C-8), 135.0 (C-5), 123.1 (CH-6), 117.9 (CH-7), 111.2 (CH_2-19), 88.3 (C-25), 72.10 (CH-1), 67.51 (CH-3),56.42(CH-14) , 56.2(CH-17), 46.1 (CH2), 45.8 (CH_2), 44.8 (CH2), 41.4 (CH_2),40.6 (C-13), 35.9 (CH_2), 35.7 (CH_3), 28.9 (CH_2), 27.72 (CH_2), 25.87 (CH_3-^{t}Bu),25.82 (CH_3-^{t}Bu), 23.49 (CH_2), 22.13 (CH_2), 20.77 (CH_2), 18.72(C-^{t}Bu), 18.23 (CH_3-^{t}Bu), 18.13 (CH_3-18), 11.97 (CH_3-21), -4.68 (CH_3-Si), -4.68 (CH_3-Si), -4.78(CH_3-Si), -5.07 (CH_3-Si).

MS (ESI)[m/z, (%)]: 658 (2), 542 (M+ - TBSO, 100), 413 (M+ - TBSO -TBSO, 14), 314 (22).

HRMS (ESI): calculated for $C_{39}H_{71}NO_4Si_2$: 673.4989, found: 673.4973.

(R)-6-{(1R,3aS,7aR,E)-4-[(Z)-2-((3S,5R)-3,5-bis((tert-butyldimethylsilyl)oxy)-2-methylenecyclohexylidene]ethylidene}-7a-methyloctahydro-1H-inden-1-yl)-2-methylheptan-2-amine (5)

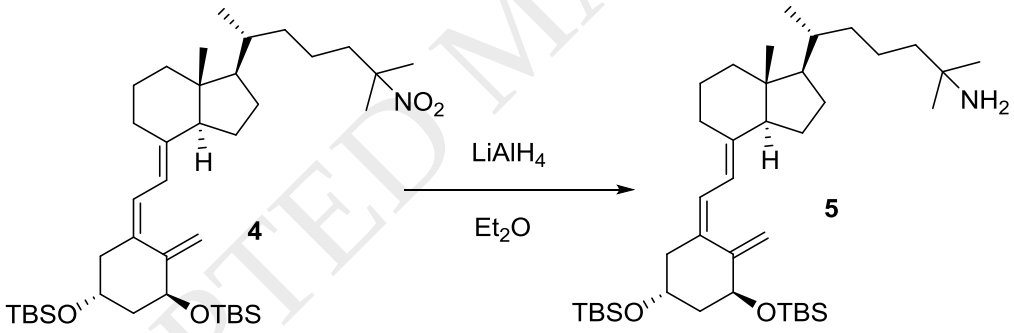

To a solution of compound **4** (164 mg, 0.24 mmol) in dry Et_2O (12 mL) at 0 ºC was added $LiAlH_4$ (90 mg, 1.217 mmol). The mixture was heated at 45 ºC for 5 h then allowed to reach room temperature. H_2O (5 mL) was added dropwise at 0 ºC and the mixture extracted with EtOAc (3 x 10 mL). The combined organic phases were dried (Na_2SO_4), filtered and concentrated under vacuum, affording a residue which was chromatographed on silica gel using 40% EtOAc/hexane as eluent, affording compound **5** (123 mg, 78%) as a colourless liquid.

Compound **5**: Rf: 0.32 (10% MeOH/ EtOAc); IR (NaCl, cm^{-1}): 3352, 3300, 2924, 2871, 1531, 1281, 1229, 1212, 1040, 986, 743, 626; $[\alpha]^{23}_D$ =-32.1 (c 1, CH_3Cl).

^{1}H-NMR ($CDCl_3$, δ): 7.1 (2H, br s, NH_2), 6.24 (1H, d, J = 11.1 Hz, H-6), 6.02 (1H, d, J = 11.1 Hz, H-7), 5.18 (1H, br s, H-19), 4.87 (1H,br s, H-19), 4.37 (1H, s, H-1), 4.18 (1H, s, H-3), 2.82 (1H, d, *J* = 7.8 Hz), 2.45 (1H, m), 2.17 (2H, m), 1.88 (9H, m), 1.51 (14H, m), 1.29 (3H, s, CH_3-26), 1.25 (3H, s, CH_3-27), 0.92 (3H, CH_3-21) 0.88 (18H, C-^{t}Bu-Si), 0.52 (3H,s, CH_3-18), 0.08 (6H, s, CH_3-Si), 0.07 (6H, s, CH_3-Si).

^{13}C-RMN ($CDCl_3$, δ): 148.26(C-10), 140.94(C-8), 134.94(C-5), 123.16(CH-6), 117.89(CH-7), 111.23 (CH_2-19), 72.12(CH-1), 67.51(CH-3), 56.59(CH-14), 56.31(CH-17), 53.21(C-25), 46.05(CH_2), 44.80(CH_2), 41.35(CH_2), 40.63(CH_2), 36.21(CH_2),36.11(CH-20), 31.92(CH_2), 29.76(CH_2), 29.37(CH_2), 28.86(CH_2), 27.78(CH_2), 25.85(CH_2), 25.81(CH_3-^{t}Bu), 25.58 (CH_3-^{t}Bu), 23.49 (CH_2), 22.68 (CH_2), 22.15 (CH_2), 20.63 (CH_2), 18.81(C-^{t}Bu), 18.21 (C-^{t}Bu), 14.12 (CH_3-18), 11.95 (CH_3-21), -4.66 (CH_3-Si), -4.69 (CH_3-Si), -4.80 (CH_3-Si), -5.09 (CH_3-Si).

MS (ESI) [m/z, (%)]: 512 (M^+ - TBSO, 100), 354 (35), 248 (7), 173 (2)

HRMS (ESI): calculated for $C_{39}H_{73}NO_2Si_2$: 643.5214, found: 643.5221.

Methyl4-{(R)-6-[(1R,3aS,7aR,E)-4-((Z)-2-((3S,5R)-3,5-bis((tert-butyldimethylsilyl)oxy)-2-methylenecyclohexylidene)ethylidene)-7a-methyloctahydro-1H-inden-1-yl)-2-methylheptan-2-yl]amino}-4-oxobutanoate (7)

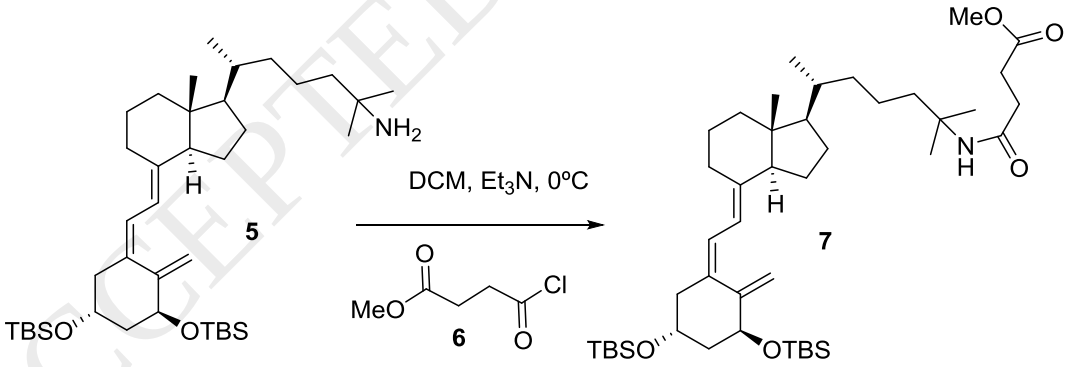

To a solution of amine **5** (90 mg, 0.140 mmol) in dry CH_2Cl_2 (5 mL) at 0 ºC was added a solution of acid chloride **6** (28 mg, 0.182 mmol) and Et_3N (46 μL) in dry CH_2Cl_2 (5 mL). The mixture was stirred for 1 h and quenched with 10% aqueous solution of $NaHCO_3$ (25 mL). The aqueous layer was extracted with CH_2Cl_2 (3 x 5 mL) and the combined organic phases were dried over Na_2SO_4, filtered, and

concentrated *in vacuo* to give, after flash column chromatography on silica gel (30% EtOAc/ hexanes), pure **7** (92 mg, 92%) as a colourless oil.

Compound **7**: Rf: 0.62 (50% EtOAc/Hexane); IR (NaCl, cm^{-1}): 3256, 2923, 2853, 1745, 1723, 1547, 1440, 1326, 1258, 1200, 1147, 956, 784; $[\alpha]^{23}_{D}$= +36.8 (c 1, CH_3Cl).

^{1}H-NMR ($CDCl_3$, δ): 6.24 (1H, d, *J* = 11.1 Hz, H-7), 6.02 (1H, d, *J* = 11.1 Hz, H-6), 5.46 (1H, s, NH), 5.17 (1H, s, H-19), 4.86 (1H, s, H-19), 4.36 (1H, m, H-3), 4.18 (1H, m, H-1), 3.69 (3H, s, OCH_3), 2.81 (2H, m), 2.64 (4H, t, *J* = 6.7 Hz), 2.47-2.05 (5H, m), 2.07-1.68 (6H, m), 1.72-1.37 (7H, m), 1.29 (3H, s, CH_3-26), 1.25 (3H, s, CH_3-27), 0.79 (21H, s, C-^{t}Bu-Si, CH_3-21), 0.53 (3H, s, CH_3-18), -0.01 (12H, s, CH_3-Si).

^{13}C-RMN ($CDCl_3$, δ): 173.61 (C-30), 170.61 (C-27), 148.26 (C-10), 141.03 (C-8), 134.91 (C-5), 123.17 (CH-6), 117.86 (CH-7), 112.0 (CH_2-19), 72.09 (CH-3), 67.51(CH-1), 56.65(CH-14), 56.32(CH-17), 53.85(C-25), 51.74(C-13), 45.77(CH_2), 44.79 (CH_2), 40.75 (CH_2), 40.70 (CH_2), 36.13(CH_3O), 31.90(CH_2), 29.68(CH_2), 29.43 (CH_2), 28.86 (CH_2), 27.71 (CH_2), 26.89 (CH_3-27), 25.85 (CH_3-26), 25.80 (CH_3-^{t}Bu-Si), 23.50 (CH_2), 22.13 (CH_2), 18.75 (CH_2), 18.22 (C-^{t}Bu-Si), 18.13 (C-^{t}Bu-Si), 11.98 (CH_3-18), -4.70 (CH_3-Si), -4.80 (CH_3-Si), -5.10 (CH_3-Si), -5.10 (CH_3-Si).

MS (ESI)[m/z, (%)]: 757 (M^+, 62), 756 (M^+ - 1, 100), 595 (M^+ - TBSO - OMe, 12), 314 (22).

HRMS (ESI): calculated for $C_{44}H_{79}NO_5Si_2$: 757.5531, found: 757.5529.

4-{(R)-6-[(1R,3aS,7aR,E)-4-((Z)-2-((3S,5R)-3,5-bis((tert-butyldimethylsilyl)oxy)-2-methylenecyclohexylidene)ethylidene)-7a-methyloctahydro-1H-inden-1-yl)-2-methylheptan-2-yl]amino}-4-oxobutanoic acid (8)

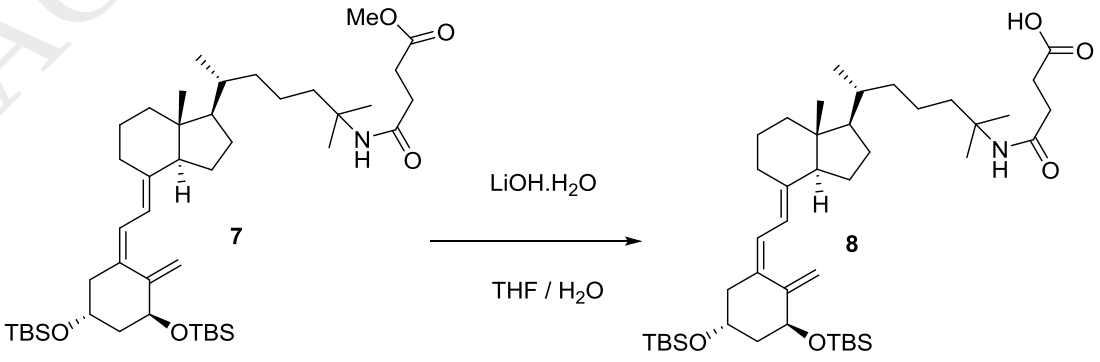

$LiOH \cdot H_2O$ (8.31 mg, 0.198 mmol) was added to a solution of **7** (100 mg, 0.132 mmol) in a mixture of THF (15 mL) and H_2O (1.5 mL). The mixture was stirred at room temperature for 16h. The pH of the mixture was adjusted to 7 with HCl (2%). The aqueous layer was extracted with EtOAc (3 x 10 mL). The combined organic phases were dried, filtered and concentrated *in vacuo*. The residue was purified by flash column chromatography (70% EtOAc/Hexanes) to give **8** (75 mg, 76%), as a colourless oil.

Compound **8:** Rf: 0.19 (50% EtOAc/Hexane); IR (NaCl, cm^{-1}): 3401, 3257, 2985, 2853, 1784, 1753, 1455, 1323, 1201, 1185, 923; $[\alpha]^{23}_{D}$= +36.7 (c 1, CH_3Cl).

^{1}H-NMR ($CDCl_3$, δ): 6.25 (1H, d, *J* = 11.2 Hz, H-7), 6.03 (1H, d, *J* = 11.2 Hz, H-6), 5.58 (1H, s, NH), 5.19 (1H, s, H-19), 4.88 (1H, s, H-19), 4.38 (1H, m, H-3), 4.20 (1H, m, H-1), 2.83 (1H, m,), 2.66 (2H, m), 2.45 (2H, m), 2.25 (1H, m),1.97-1.43 (17H, m), 1.31 (6H, s, CH_3-27 and CH_3-26), 0.89 (18H, s, C-^{t}Bu-Si), 0.54 (3H, s, CH_3-18), 0.08 (12H, s, CH_3-Si).

^{13}C-RMN ($CDCl_3$, δ): 176.2 (C-30), 171.7 (C-27), 148.3 (C-10), 141.0 (C-8), 134.9 (C-5), 123.2 (CH-6), 117.9 (CH-7), 112.0 (CH_2-19), 72.5 (CH-1) 67.5 (CH-3), 56.6 (CH-14), 56.3 (CH-17), 56.4 (C-25), 46.8 (C-13) 45.8 (CH_2), 44.8 (CH_2), 40.6 (CH_2), 40.4 (CH_2), 36.1 (CH-20),36.0 (CH_2) 31.6 (CH_2), 29.6 (CH_2), 28.9 (CH_2), 27.7 (CH_2), 26.7 (CH_3-26 o CH_3-27), 26.6 (CH_3-26 o CH_3-27), 25.9 (CH_3-^{t}Bu-Si), 25.8 (CH_3-^{t}Bu-Si), 23.5 (CH_2), 22.4 (CH_2), 21.2 (), 20.6 (CH_2), 18.2 (C-^{t}Bu-Si), 18.2 (C-^{t}Bu-Si), 14.2 (CH_3-21), 12.0 (CH_3-18), -4.6 (CH_3-Si), -4.7 (CH_3-Si), -4.8 (CH_3-Si), -5.1 (CH_3-Si).

MS (ESI) [m/z, (%)]: 766 (M^+ + Na, 100), 649 (52), 426 (21).

HRMS (ESI): calculated for $C_{43}H_{77}NaNO_5Si_2$: 766.5341, found: 766.5336.

4-{(R)-6-[(1R,3aS,7aR,E)-4-((Z)-2-((3S,5R)-3,5-dihydroxy-2-methylenecyclohexylidene)ethylidene)-7a-methyloctahydro-1H-inden-1-yl)-2-methylheptan-2-yl]amino}-4-oxobutanoic acid (ML-344)

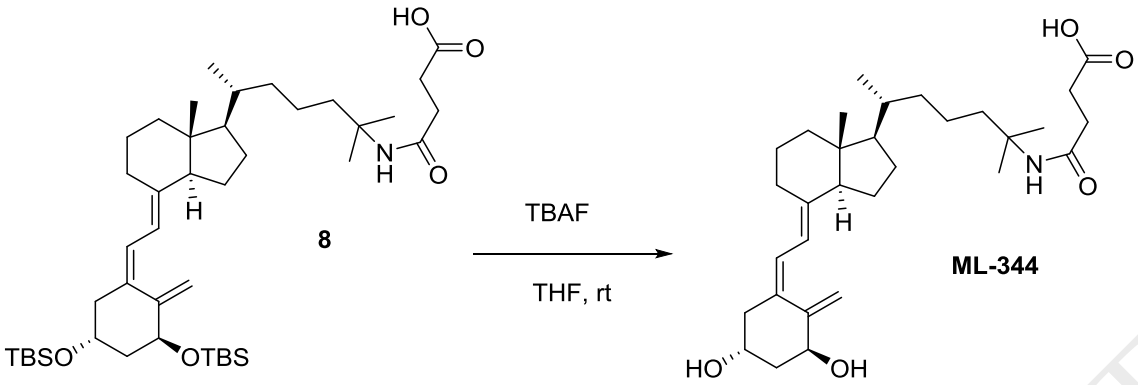

Tetrabutylammonium fluoride (246 µL, 0.246 mmol, 1M solution in dry THF) was added to a solution of **8** (45 mg, 0.062 mmol) in dry THF (4 mL). The reaction mixture was stirred in the dark for 4 h. Water (4 mL) was added and the aqueous layer was extracted with Et_2O (3x10 mL). The combined organic phases were dried, filtered and concentrated *in vacuo*. The residue was purified by flash column chromatography (50% EtOAc/Hexanes) to give target compound **ML-344** (23 mg, 76%).

Compound ML-344: Rf: 0.08 (70% EtOAc/Hexane); IR (NaCl, cm^{-1}): 3440, 3313, 3265, 3202, 2985, 2853, 1745, 1740, 1485, 1278, 1202, 1156, 854, 652.; $[\alpha]^{30}_D$= +14.3 (c 1, CH_3Cl).

^{1}H-NMR ($CDCl_3$, δ): 6.40 (1H, d, *J* = 11.3 Hz, H-7), 6.03 (, d, *J* = 11.3 Hz, H-6), 5.52 (1H, s, NH), 5.33 (1H, s, H-19), 5.02 (1H, s, H-19), 4.45 (1H, m, H-3), 4.25 (2H, m, H-1), 3.33 (2H, m), 2.98 (1H, m), 2.83 (1H, m), 2.65 (4H, m), 2.50 (2H, m), 2.33 (2H, m), 1.72-1.43 (24H, m), 1.33 (6H, s, CH_3-27 and CH_3-26), 0.98 (3H, d, *J* = 6.3Hz, CH_3-21), 0.56 (3H, s, CH_3-18).

^{13}C – NMR ($CDCl_3$, δ): 174.4 (C-30), 174.3 (C-27).149.9 (C-10), 142.6 (C-8), 135.7(C-5), 124.9 (CH-6), 119.0 (CH-7), 112.1 (CH_2-19), 71.5 (CH-1), 67.4 (CH-3), 58.1 (CH-14), 57.6 (CH-17), 54.9 (C-25), 54.6 (C-13), 47.0 (CH_2), 46.2 (CH_2), 43.7 (CH_2), 42.0 (CH_2), 41.3 (CH_2), 37.5 (CH_2), 37.4 (CH-20), 33.0 (CH_2), 30.0 (CH_2), 28.8 (CH_2), 27.4 (CH_3-26 y CH_3-27), 24.7 (CH_2), 24.6 (CH_2), 23.3 (CH_2), 21.7 (CH_2), 19.4 (CH_3-21), 12.4 (CH_3-18).

MS (ESI)[m/z, (%)]: 538 (M^+ + Na, 100), 414 (62), 389 (36), 126 (3).

HRMS (ESI): calculated for $C_{31}H_{49}NaNO_5$: 538.3611, found: 538.3636.

4.1.2. ^{1}H and ^{13}C spectra

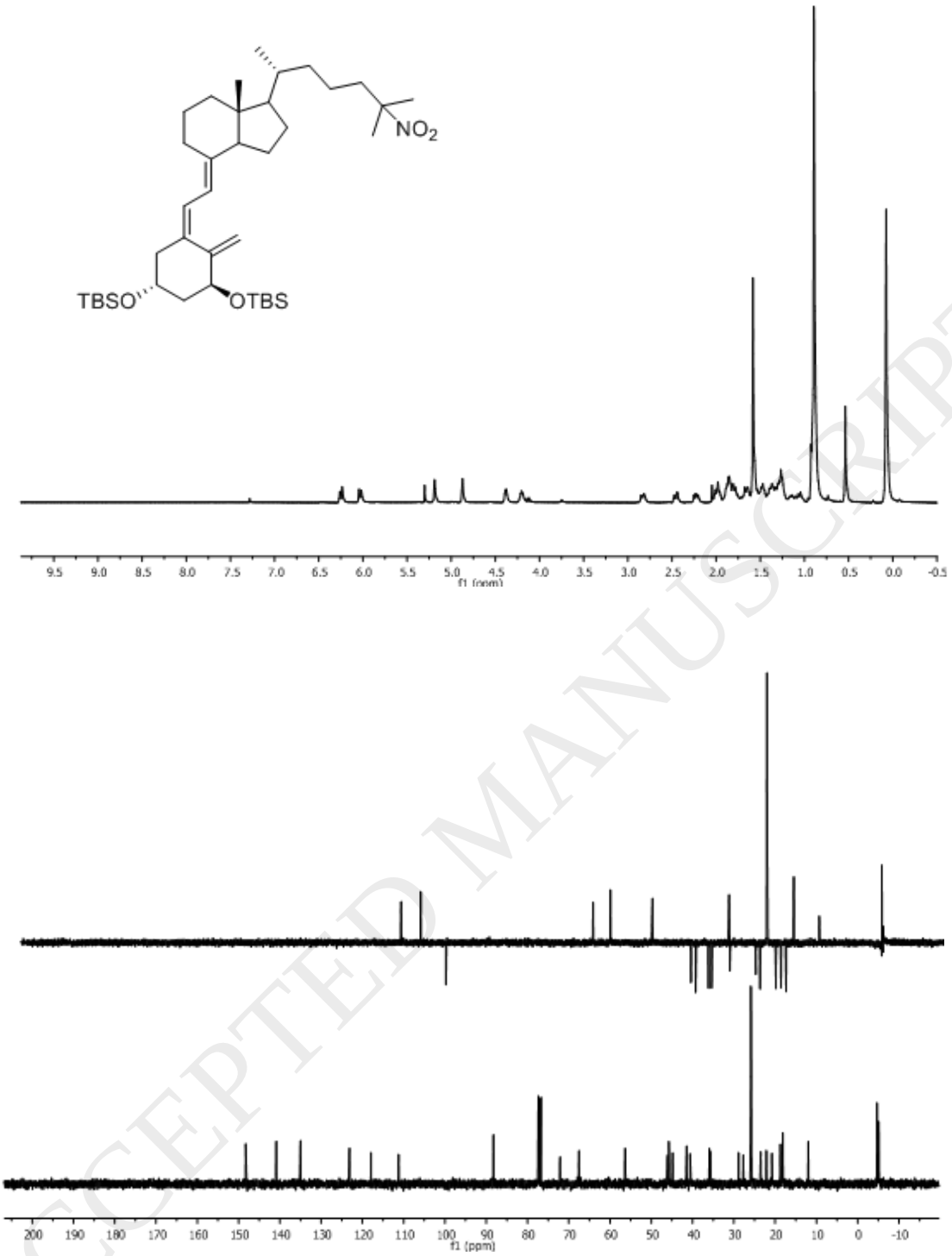

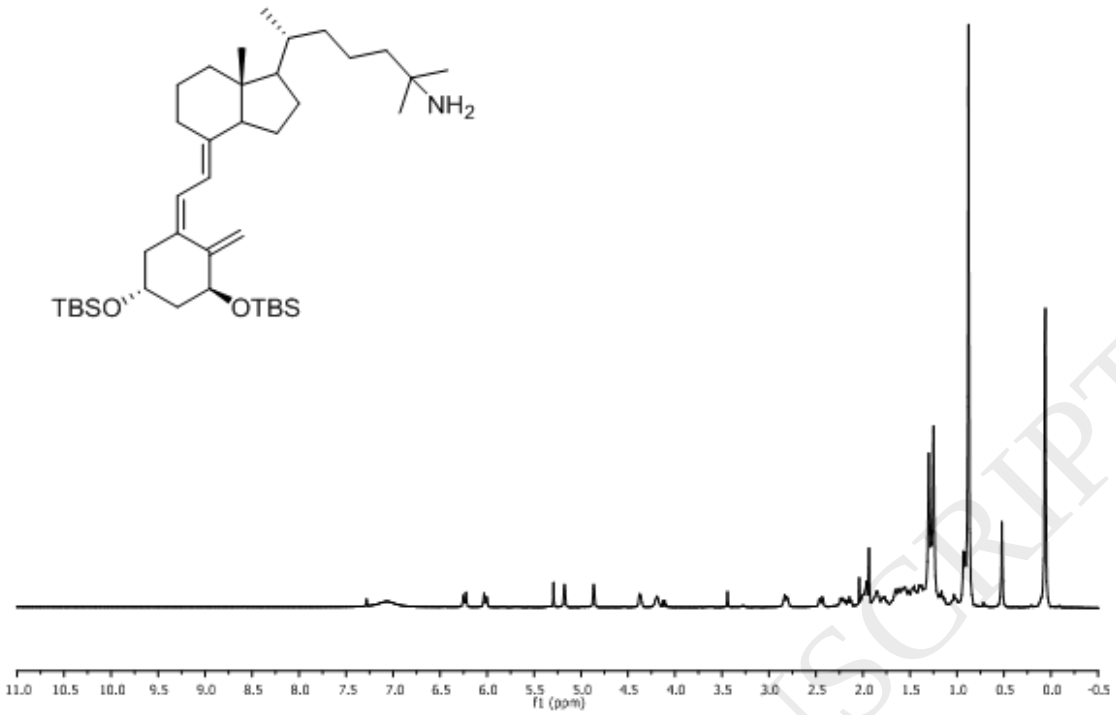

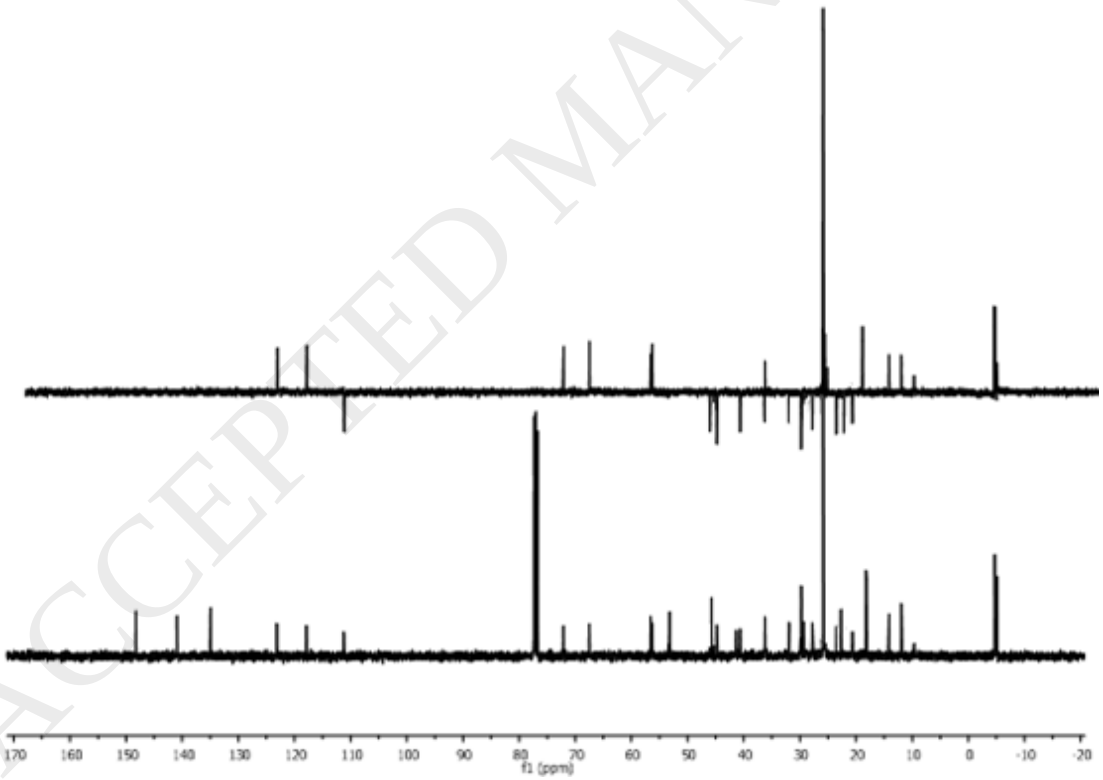

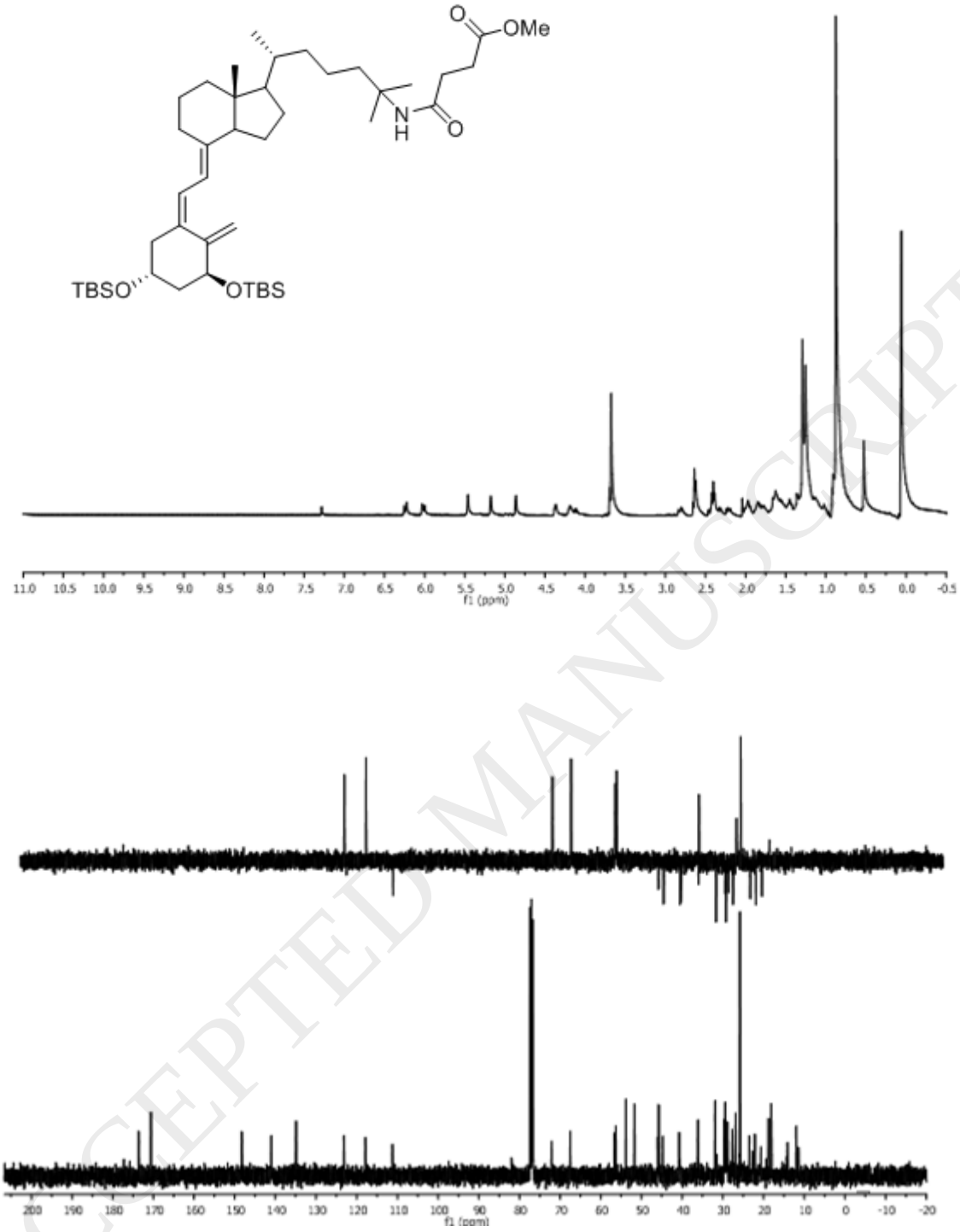

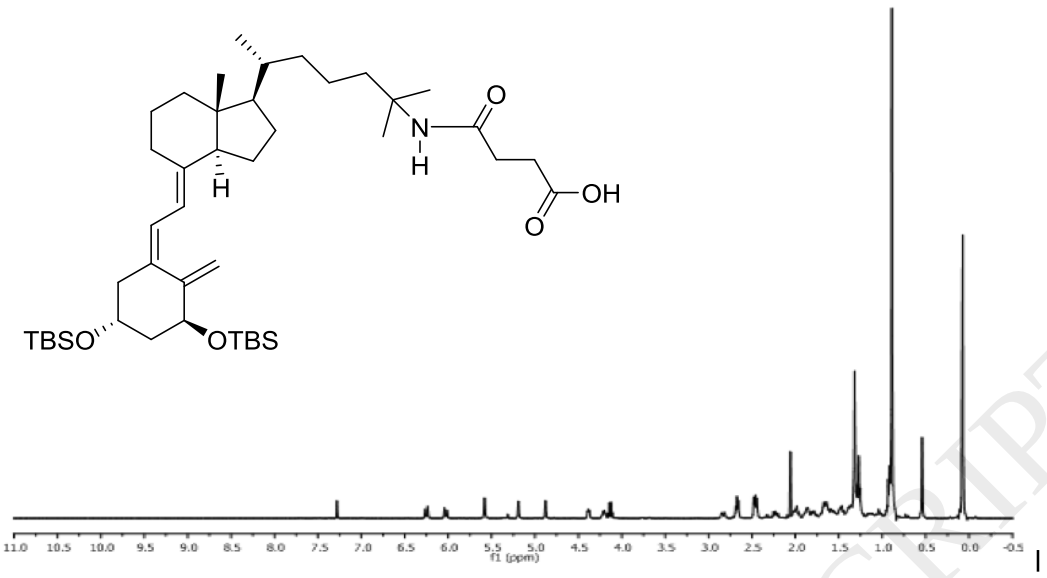

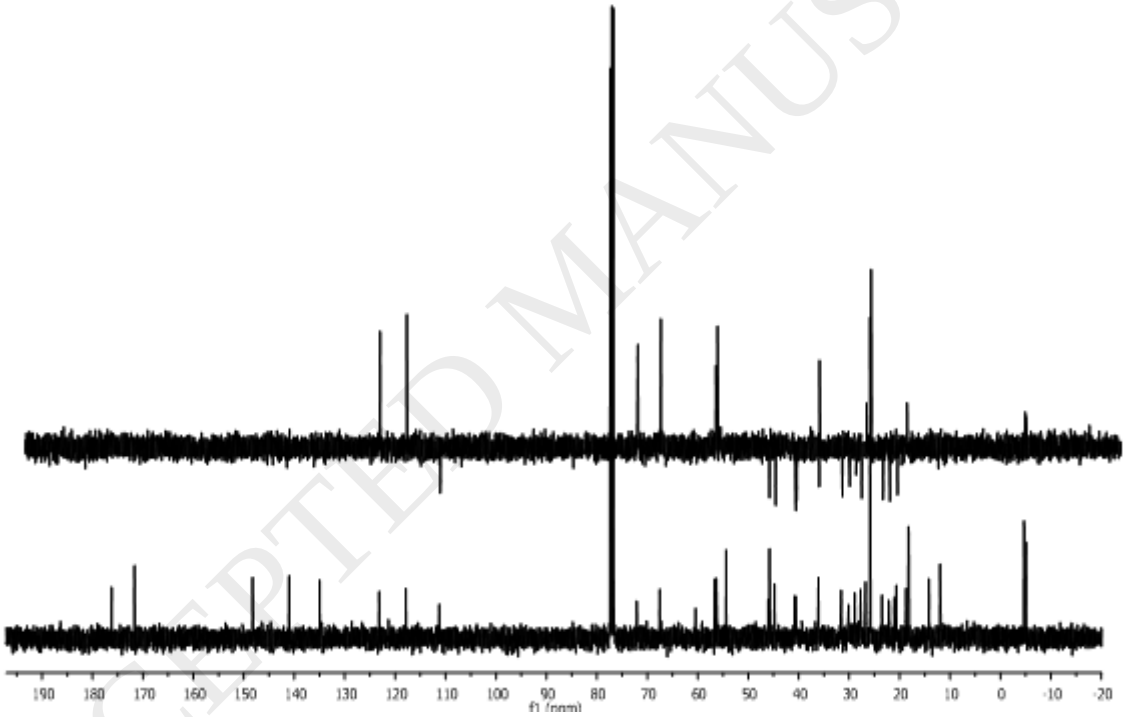

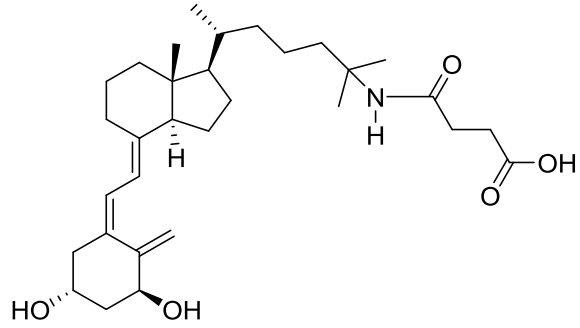

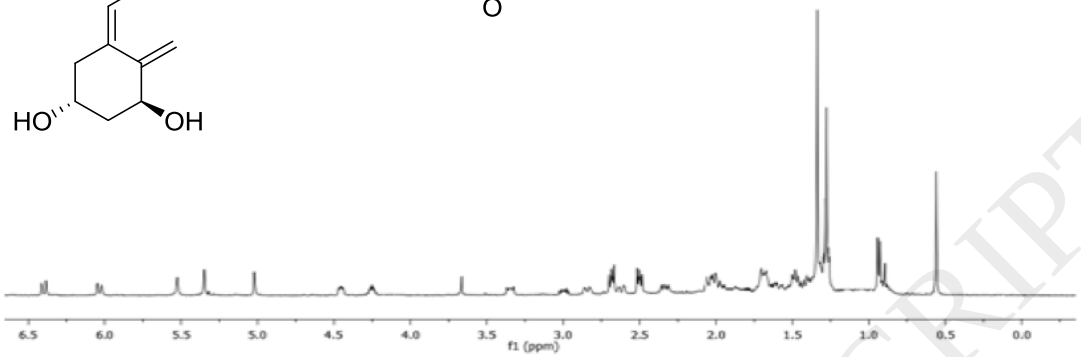

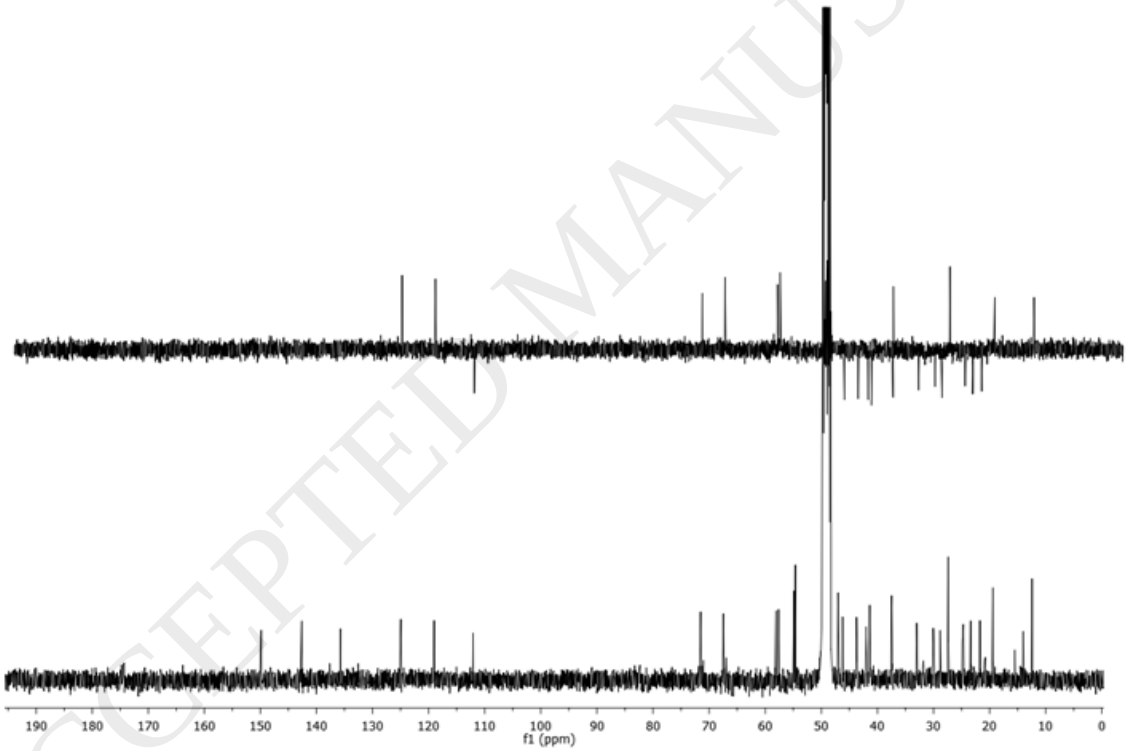

2.2. BIOLOGICAL ASSAYS

2.2.1. Cell viability assay

Cells were cultured in 96-well plates and treated with vehicle (isopropanol), ML-344 analog or calcitriol at the concentration range of 10^{-11} to 10^{-7} M for 120 h, replacing the medium every 2 days. Cell viability was assessed by using WST-1

colorimetric assay (Roche) and cell counting. To this end, following treatments of the cells, they were incubated for 1 h at 37 ºC with the tetrazolium salt (4-[3-(4-Iodophenyl)-2-(4- nitrophenyl)-2H-5-tetrazolio]-1,3 benzene disulfonate) and the absorbance of the formazan product was read at 440 nm and 690 nm (reference wavelength). Then, cells were washed with PBS 1X, trypsinized, suspended in 100 µl of complete medium and counted manually using a hemocytometer. Each treatment was performed in quadruplicate and the experiment was repeated three times.

2.2.2. Analysis of cellular DNA content by flow cytometry

Propidium iodide (PI) was used for DNA staining to determine the percentage of cells in each phase of the cell cycle. Approximately 1×10^4 4T1 cells were seeded in 35 mm cell culture dishes and kept at 37 °C, 5% CO_2 for 48 h. Then, the cells were treated with 100 nM of ML-344 or vehicle during 96 h. The cells were detached, centrifuged, washed twice with ice-cold PBS 1X, fixed in 70% cold ethanol, and stored at -20 °C during 24 h. Then, the cells were centrifuged, washed with PBS 1X and stained by PI (50 µg/mL, Roche) and RNase A (100 µg/mL) to degrade double-stranded RNA in PBS 1X and incubated at 37 °C for 30 min. Flow cytometry analysis was performed using FACS Calibur (Becton Dickinson). One thousand events were analyzed for each sample.

2.2.3. Cell migration assay

Cell migration was evaluated by “wound healing” assays, as previously described [9]. In brief, a confluent monolayer of cells was scratched with a pipette tip and the medium was discarded to remove the floating cells. Then, fresh medium containing vehicle, ML-344 or calcitriol (100 nM) was added to each plate. Images of cell migration into the wound were captured over the time employing the microscope NIKON ECLIPSE TE 2000S, equipped with the digital camera Nikon Coolpix S4, 6.0 Mpix, 10x zoom. The time of the experiments does not exceed the doubling time of each cell line evaluated. The area of the wounds was quantified using ImageJ 1.37 v (NIH) software. The experiment was repeated three times.

2.2.4. Cell invasion assay

Invasion ability of cancer cells was evaluated by Matrigel-coated Transwell inserts (Millipore) as previously described [10]. The inserts were seeded in 24-well cell culture plates that were filled with 600 µL of complete medium as a chemo-attractant. The upper surfaces of 12-µm pore size polycarbonate inserts were coated with 100 µl of Matrigel (BD Biosciences), diluted 1:3 in serum-free medium, and incubated at 37 °C to solidify the Matrigel for 30 min. Then, the cells were seeded into the upper part of the Matrigel-coated filters (12.5×10^3 cells in 400 µl / insert) and incubated with vehicle or ML-344 (100 nM). After incubation for 12 h, invading cells of the bottom of the inserts were fixed in 100% methanol for 10 min at room temperature and stained with crystal violet. The experiments were performed in triplicate and ten randomly fields from each insert were photographed and counted with ImageJ software.

2.2.5. Actin cytoskeleton analysis by rhodamine-phalloidin staining

Immunofluorescence was performed as previously described [10]. Briefly, LM3 cells were seeded on glass coverslips ($9x10^4$) in 35 mm Petri dishes and cultured until 60% confluence. They were treated with the analog (100 nM) or vehicle for 16 h. After treatment, they were washed three times with PBS 1X and fixed with paraformaldehyde 4% in PBS 1X for 1 h. The cells were then permeabilized with 0.1% triton in PBS 1X and incubated with rhodamine-phalloidin (1:100) in PBS 1X for 30 min and To-pro3 (1:1000) in PBS 1X for 5 min. After that they were washed three times with PBS 1X and glass coverslips were mounted on glass microscope slides. Fluorescence images were acquired with the Leica confocal microscopy TSP2 and analyzed with ImageJ software. The total number of cells per field and stress fibers-containing cells were counted in 10 randomly chosen fields of each sample. The experiment was performed in triplicate.

2.2.6. Effects of ML-344 on blood calcium levels

All animal studies were performed in accordance with ARRIVE guidelines and the three Rs rule of replacement, reduction and refinement principles. The animals were treated according to protocols approved by the CICUAE (Institutional Committee for the Care and Use of Experimental Animals) at the Universidad Nacional del Sur, Bahía Blanca, Argentina, and conducted in

accordance with the NIH Guide for the Care and Use of Laboratory Animals. Male inbred normal CF1 mice (8 –10 weeks of age, 40 g of weight) provided by Departamento de Biología, Bioquímica y Farmacia (Universidad Nacional del Sur, Bahía Blanca, Argentina) were employed to analyze plasma calcium levels following a 5 µg/Kg body weight dose of the ML-344 analog. Mice were randomly divided into two groups and were intraperitoneally injected with ML-344 (n=5), calcitriol (n=5) or vehicle (n=6) with nine total doses (five consecutive doses in one week and four consecutive doses in the following week). Body weight was evaluated during treatment period. Plasma calcium levels were determined as previously described [11]. Briefly, blood samples were collected from mice (basal levels as well as at 24, 48, 72, 96, 264 h) in heparinized tubes and centrifuged to calculate the hematocrit from each mouse. Then, the plasma fraction was separated and employed to determine total calcium levels using Ca-Color Arsenazo III AA kit (Wiener Lab, Argentina). In addition, ionized calcium levels were calculated by a correction with total protein content of the sample and measured using a COBAS C311 analyzer (Roche Diagnostics). These studies were carried out at Gama Clinical Laboratories (Bahía Blanca), which routinely performs these analyses on human samples.

2.3. COMPUTATIONAL STUDIES

Molecular docking studies were performed using as receptor template the crystallographic structure of VDR deposited under the code PDB: 1DB1 in the Protein DataBank [12]. Before performing docking studies, the receptors were parameterized using the *ff14SB* forcefield [13], with the corresponding ionization states of tritable residues being assigned both at pH 5.5 and 7. The structure of the corresponding ligands (i.e. calcitriol and ML-344) were constructed using MarvinSketch software [14], and afterwards subjected to energy minimizations using and *ab initio* (HF/6-311+G*) method as implemented in Gaussian09 [15]. Ligands subjected to docking studies were parameterized using the GAFF2 forcefield [16], with charges being assigned by applying the AM1-BCC fitted charges [17].

Docking procedures were conducted using software developed by OpenEye Scientific Software [18] by applying the following protocol: a) a library of ligand conformers was generated at an energy threshold of 10 Kcal/mol using

the OMEGA conformer generator [19,20]. In a second stage, b) conformer libraries were docked to the corresponding receptors, using the fast rigid exhaustive docking method implemented in the FRED3 software [21,22]. The evaluation and ranking of the corresponding docked poses was performed based on the ChemGauss3 scoring function, selecting the lowest energy docked conformation for further analyses. Three dimensional visualization and depiction of intermolecular contacts was performed using the VIDA and LigPlot+ software, respectively [23,24].

Molecular dynamics (MD) simulations were performed under explicit solvent conditions using the AMBER16 suite of software [25,26]. As was done for docking runs, ligands and receptors parameters were assigned from the *GAFF2* and *ff14SB* forcefields, respectively. System preparation and parameterization was performed using the *tLeap* module of the AMBER16 software suite. Simulation trajectories were obtained applying periodic boundary conditions, constructing cubic boxes of explicit preequilibrated TIP3P water molecules, with a minimum distance of 12 Å between the box edges and the solute. In order to obtain the corresponding trajectories, a previously validated MD workflow was applied, as follows: a) a dual-stage minimization stage, in which water molecules were initially minimized with the solute being constrained, followed by a whole system minimization (10000 steps of minimization for each stage). Next, a b) heating stage was applied, thermostatizing the system from 0 to 297 K during 500 ps, and followed by c) an equilibration phase for additional 2 ns. Finally, d) the equilibrated systems were subjected to production runs (80 ns) obtained under constant pressure and temperature conditions, using a time step of 2 fs and the SHAKE algorithm in order to constrain bonds involving hydrogen atoms. Simulation convergence was checked by means of structural and energetic inspection using the Cpptraj module of AMBER16. Finally, overall and per-residue energetic analysis were performed over 8000 homogenously sampled production frames using the MMPBSA.py script [27, 28]. Visualization of snapshots and structural properties were calculated and depicted using VMD v1.9. This work used computational resources from CCAD – Universidad Nacional de Córdoba (http://ccad.unc.edu.ar/), in particular the Mendieta Cluster, which is part of SNCAD – MinCyT, República Argentina, and using the *pmemd.cuda* module of AMBER16.

3. RESULTS

3.1. SYNTHESIS

In this work, we have designed a route for the synthesis of ML-344, a novel vitamin D analog with a nitrogen atom bonded to C-25 (Scheme 1). The design of the side chain of ML-344 is the result of our previous effort to synthesize 25-amino vitamin D_3 derivatives through the protection of the nitrogen atom as amide [29]. The use of commercially available succinic acid-derived acid chloride resulted successful, hence leading to a new vitamin D analog. Accordingly, ketone **2** was synthesized from Inhoffen diol **1** using the method developed in our laboratory [29]. The Wittig-Horner reaction of ketone **2** with phosphine oxide **3** afforded 83% yield of the desired nitro compound **4** which on reaction with lithium aluminium hydride gave amine **5** in 78% yield. Amine **5**, on reaction with acid chloride **6** afforded amide **7** in 92% yield. Compound **7** upon reaction with lithium hydroxide afforded 76% yield of acid **8**. The final desilylation of 8 occurred uneventfully affording 75% yield of the desired calcitriol analog **ML-344.**

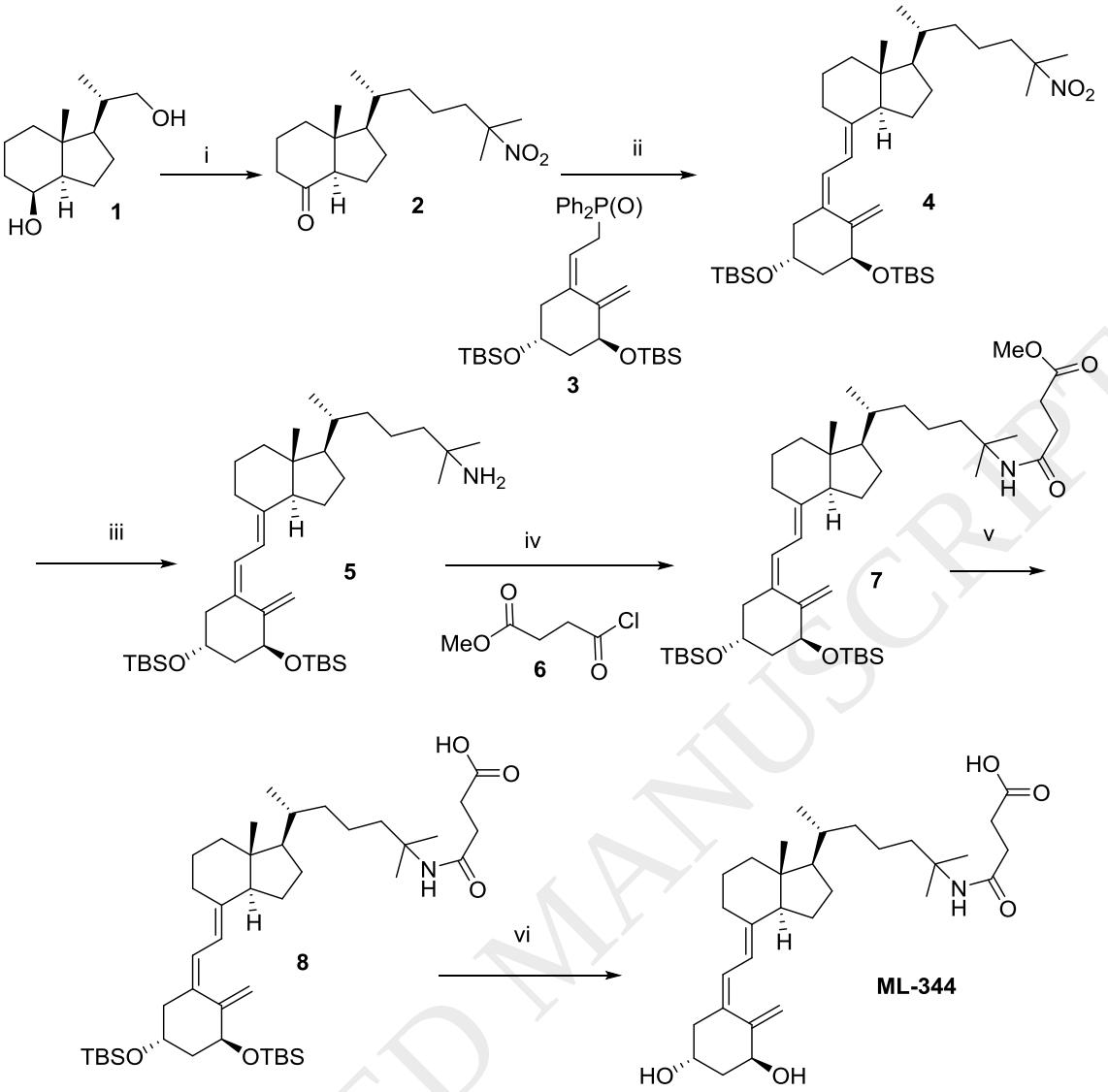

Scheme 1. Synthesis of target compound ML-344. *Reagents and conditions*: (i) see reference: Rivadulla and col. [29]; (ii) **3**, *n*-BuLi, THF, -78 ºC (83%); (iii) $LiAlH_4$, Et_2O, 45 °C (78%); (iv) **6**, CH_2Cl_2, Et_3N, 0 °C, 1 h, (92%); (v) $LiOH.H_2O$, THF/H_2O, r.t., 16 h (76%); (vi) TBAF, THF, r.t. (75%).

3.2. BIOLOGICAL EVALUATION

3.2.1. ML-344 decreases the viability of different cancer cell lines while not affecting non-malignant cells.

The effect of ML-344 on cell viability was tested on different cancer cell lines at a wide range of concentrations (10^{-11} M to 10^{-7} M) during 120 h. The effects were compared with those elicited by calcitriol. Moreover, taking into account that it has been reported that calcitriol affected the viability of normal and

non-malignant cells such as astrocytes [30] and HC11 cell line [31], we also decided to evaluate the effect of the analog on these cells.

As shown in Figure 1, both the analog and calcitriol reduced the viability of different cell lines of breast cancer, glioblastoma and head and neck squamous carcinoma. In relation to mammary cells, we tested the effects of the compounds on the viability of the LM3 hormone-independent breast cancer cell line (Fig. 1A) and on the 4T1 triple-negative breast cancer cell line (Fig. 1B). ML-344 decreased the viability of both cell lines while calcitriol only reduces the viability of the latter. Moreover, in contrast to calcitriol, it is noteworthy that no effect on the growth of HC11 non-malignant mammary epithelial cells was observed after ML-344 treatment (Fig. 1C). Regarding glioblastoma multiforme cells, the viability of the murine GL26 and human U251 cell lines was reduced by both ML-344 and calcitriol treatment (Fig. 1 D and E). Neither of the compounds affected the viability of human glioma T98G cells (Fig. 1F). An important difference between calcitriol and its analog is that ML-344 did not affect the viability of normal human astrocytes at any concentration tested (Fig. 1G). Finally, in relation to the viability of the human head and neck squamous cell carcinoma cells, ML-344 only affected HN12 cell viability while calcitriol significantly reduced that of both cell lines (Fig. 1 H and I).

Figure 1

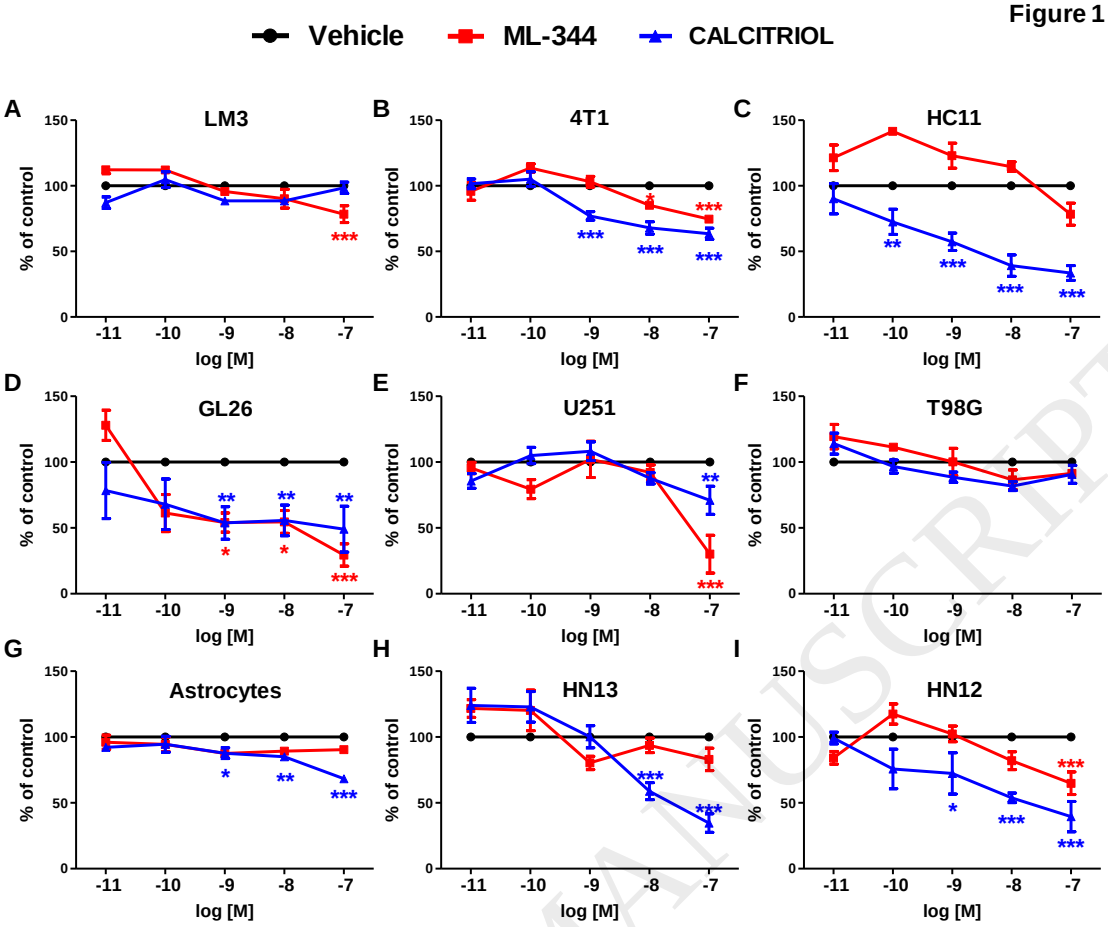

Figure 1. Effect of ML-344 analog on cell viability. Concentration-response curves obtained from **A)** LM3, **B)** 4T1, **C)** HC11, **D)** GL26, **E)** U251, **F)** T98G, **G)** Primary astrocytes, **H)** HN13 and **I)** HN12 cells exposed to vehicle, ML-344 or calcitriol over a total period of 120 h. The results were expressed as percentage of vehicle-treated cells. Data points represent mean ± SEM from three independent experiments. Two-way ANOVA and Bonferroni post-test was applied; * $p<0.05$, ** $p<0.01$ and *** $p<0.001$.

Table 1 shows the IC_{50} values obtained from cell viability assays performed with the different cells treated with ML-344 or calcitriol. They were calculated by non-linear regression.

Considering that the analog displayed strong effects on breast cancer cells, and that 4T1 is a representative cell line of triple-negative breast cancer, a subtype of tumor with limited therapeutic options, we further decided to analyze if ML-344 affects the proliferation or death of these cells. To this end, cell cycle was studied by flow cytometry using 4T1 cells treated with ML-344 (100 nM, 96 h) and labeled with Propidium Iodide (PI). As depicted in Figure 2, ML-344 treatment caused an arrest of cells in G0/G1 phase. After analog treatment the

percentage of cells in G0/G1 phase was 60.74 ± 2.04% compared to 53.53 ± 2.07% in the vehicle-treated cells (*** p<0.001); this increase of cells in G0/G1 phase was accompanied by a decrease of cells in S phase (*** p< 0.001). No changes in the sub G0/G1 population were observed. Therefore, the analog has antiproliferative effects on 4T1 breast cancer cells.

Figure 2

A

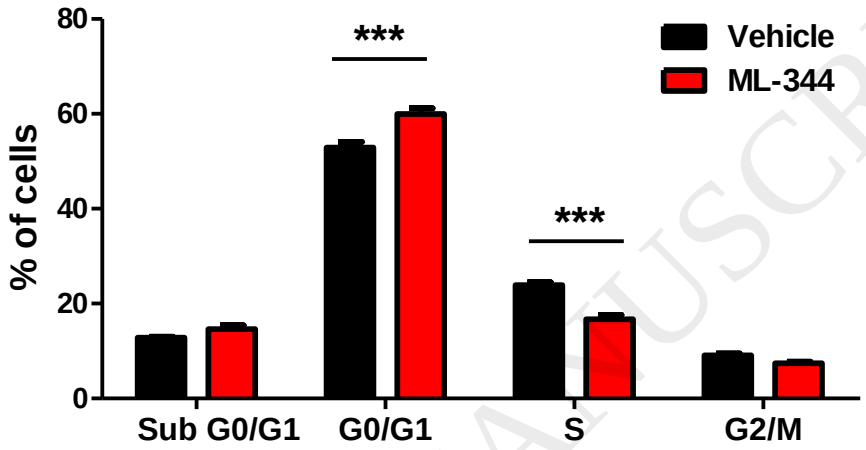

B

Table 2. Analysis of cellular DNA content by flow cytometry		
	Vehicle (%)	ML-344 (%)
Sub GO/G1	13.02 ± 0.29	14.83 ± 1.36
GO/G1	53.53 ± 2.07	60.74 ± 2.04
S	24.23 ± 0.98	16.94 ± 1.55
G2/M	9.21 ± 0.67	7.49 ± 0.65

Figure 2. Effect of ML-344 analog on cell cycle progression in breast cancer cells. 4T1 triple-negative cells were treated with ML-344 (100 nM; 96 h) and stained with PI in order to analyze the percentage of cells in the different phases of the cell cycle. **A)** The graph shows cell populations in each phase of the cell cycle. Each bar represents means ± SD (n=3). **B)** The table shows the percentage of cells in each phase of the cell cycle. Two-way ANOVA and Bonferroni post-test was applied; *** p<0.001.

3.2.2. ML-344 retards the migration of cancer cells whereas it does not affect non-malignant HC11 cells motility.

Calcitriol and its analogs modulate cell migration and invasion rates in various tumor types [1,5], so we proposed to assess whether ML-344 could affect these processes. For this purpose, we evaluated the effects of the analog and calcitriol on cell migration by “wound healing” assays employing the same cell lines that were used in cell viability assays. As depicted in Figure 3, ML-344 retarded the migration of LM3 and 4T1 breast cancer cells (Fig. 3 A and B) and U251 and T98G glioblastoma multiforme cell lines (Fig. 3 E and F). In contrast to this antimigratory activity of ML-344, calcitriol did not affect cell migration of these tumor cell lines. In murine GL26 glioblastoma multiforme cells (Fig. 3D) and HN13 and HN12 human head and neck squamous cell carcinoma cell lines (Fig. 3 G and H), the analog did not affect their migratory capacity. Finally, it is important to note that the migration of the HC11 non-malignant mammary epithelial cells was not affected after ML-344 treatment (Fig. 3C).

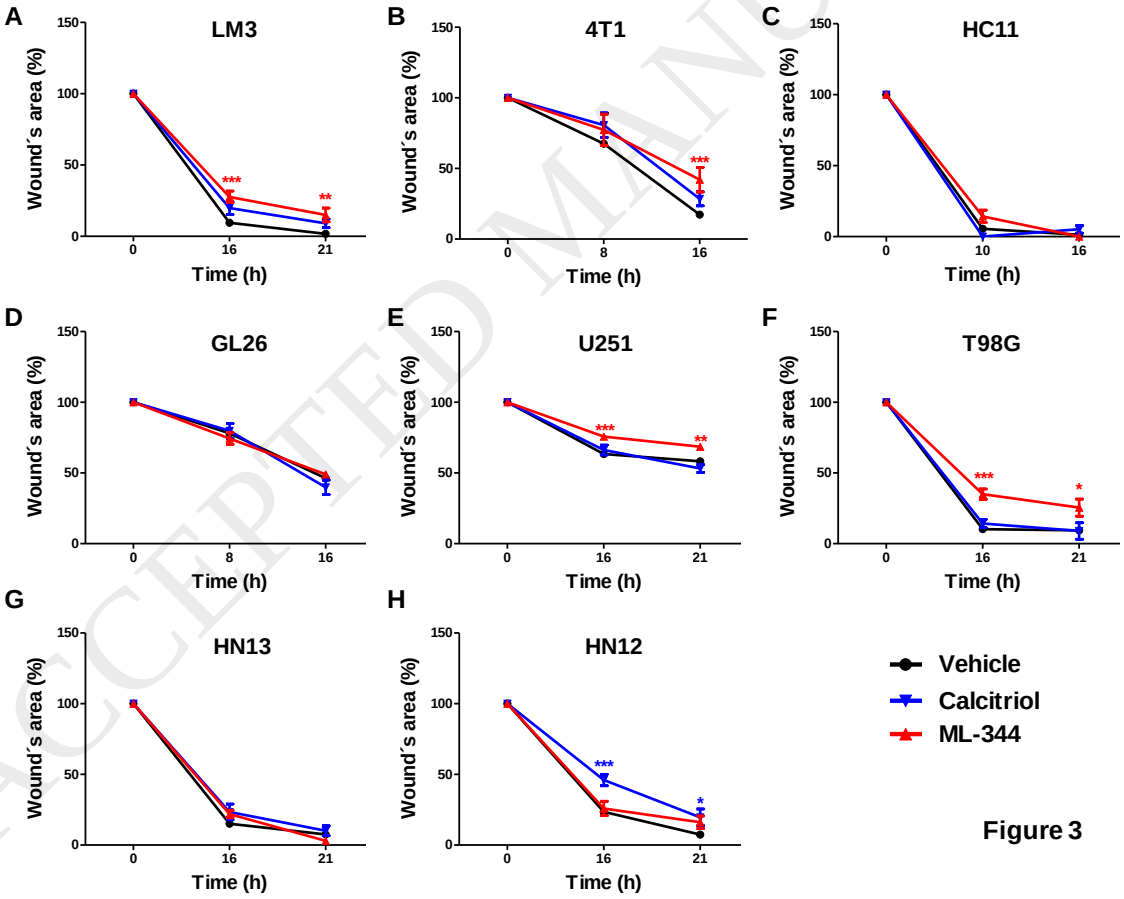

Figure 3. Effect of ML-344 analog on cell migration. Wound healing assays of the **A)** LM3, **B)** 4T1, **C)** HC11, **D)** GL26, **E)** U251, **F)** T98G, **G)** HN13 and **H)** HN12 cells treated with vehicle, ML-344 or calcitriol (100 nM). The wounds were photographed and uncovered area was quantified using ImageJ 1.37 v software. The graphs show the percentage of wound respect to time 0 h of

three independent experiments. Two-way ANOVA and Bonferroni post-test was applied; * $p<0.05$, ** $p<0.01$ and *** $p<0.001$.

3.2.3. ML-344 decreases the invasive capacity of mammary cell lines.

Based on the antimigratory activity of ML-344 on the highly invasive LM3 and 4T1 breast cancer cells and its selectivity of action between breast tumor and non-malignant cells, we continued evaluating the effects on cellular invasion. To assess this ability, Matrigel-coated transwell invasion assays were performed. As shown in Figure 4, ML-344 treatment significantly reduced the invasion rates of mammary cells compared with vehicle-treated cells. The number of LM3 invasive cells was: vehicle = 30.50 ± 1.93 vs ML-344 = 19.24 ± 3.47; ** $p=0.0047$ (Fig. 4A); the number of 4T1 invasive cells was: vehicle = 42.97 ± 2.25 vs ML-344 = 9.97 ± 0.94; *** $p<0.001$ (Fig. 4B); and the number of HC11 invasive cells was: vehicle = 23.67 ± 1.16 vs ML-344 = 16.72 ± 1.30; *** $p<0.001$ (Fig. 4C). In this case, no differences between tumor and non-malignant cells were found.

Taking into account that ML-344 affected not only the migratory but also the invasive capacity of the breast cancer cells, we decided to study the effects of the analog on the reorganization of the actin cytoskeleton, which is an important event related to the acquisition of the invasive phenotype. To this end, LM3 cells treated with vehicle or ML-344 (100 nM, 16 h) were labeled with rhodaminated phalloidin and the F-actin filaments were visualized by confocal microscopy. As shown in Figure 4D, ML-344 reduced the number of cells with stress fibers compared to the control. The percentage of cells with stress fibers in the ML-344-treated cells was 8.66 ± 6.49% compared to 91.33 ± 6.50% found in vehicle-treated cells; *** $p<0.001$. These results suggest that the analog induces a rearrangement of the actin cytoskeleton thus inhibiting the breast metastatic phenotype.

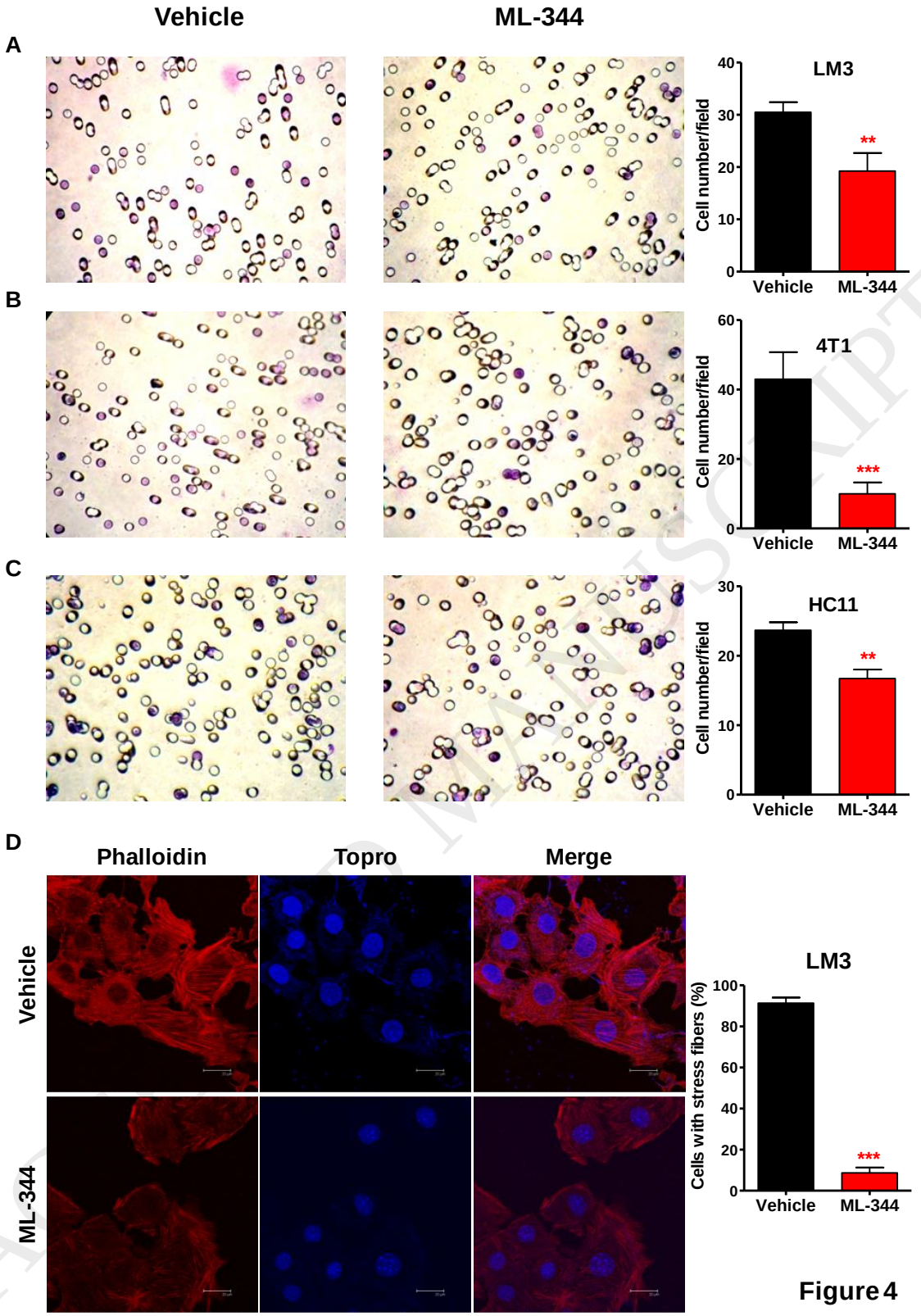

Figure 4. Effect of ML-344 analog on the mammary invasive phenotype. Breast cancer **A)** LM3 and **B)** 4T1 cells, and non-malignant **C)** HC11 cells were seeded into Matrigel-coated transwell inserts and treated with vehicle or ML-344 (100 nM). The underside of the inserts was stained 12 h after cell loading with crystal violet. The assays were performed in triplicate and invading cells were scored from 10 random fields from each insert. Representative images are shown (magnification, ×400). The graphs show the mean ± SD of the invasive cells per field. **D)** Effect of ML-344 analog on the reorganization of actin fibers in LM3 cell line. The cells were

treated with vehicle or ML-344 (100 nM, 16 h). The graph shows the percentage of cells with stress fibers. Each bar represents the average of 10 randomly chosen fields. The experiment was conducted in triplicate. Representative confocal images are shown (magnification, ×630, scale bar: 20 µm). Unpaired t-test was applied, ** $p<0.01$ and *** $p<0.001$.

3.2.4. ML-344 does not cause hypercalcemic effects in CF1 mice.

It is well known that the therapeutic application of calcitriol as an antitumor agent is hampered by its risk of inducing hypercalcemic effects. In order to evaluate the calcemic activity of the novel analog, ML-344 was administered at continuous doses of 5 µg/Kg of body weight by intraperitoneal injections in CF1 mice. The effects of the analog on plasma calcium levels, hematocrit and body weight are depicted in Figure 5 and are compared to those elicited by calcitriol. After administration of ML-344, both the total and ionized calcium remained within normal levels (Fig. 5 A). The hematocrit of ML-344- treated mice remained within normal levels (Fig. 5 B) and the body weight did not change significantly with respect to vehicle-treated mice during all the treatment period ($p > 0.05$; Fig. 5C). Instead, calcitriol produced an increase in total and ionized calcium and decreased the body weight, provoking the death of the animals following 72 h, as previously described [9, 11].

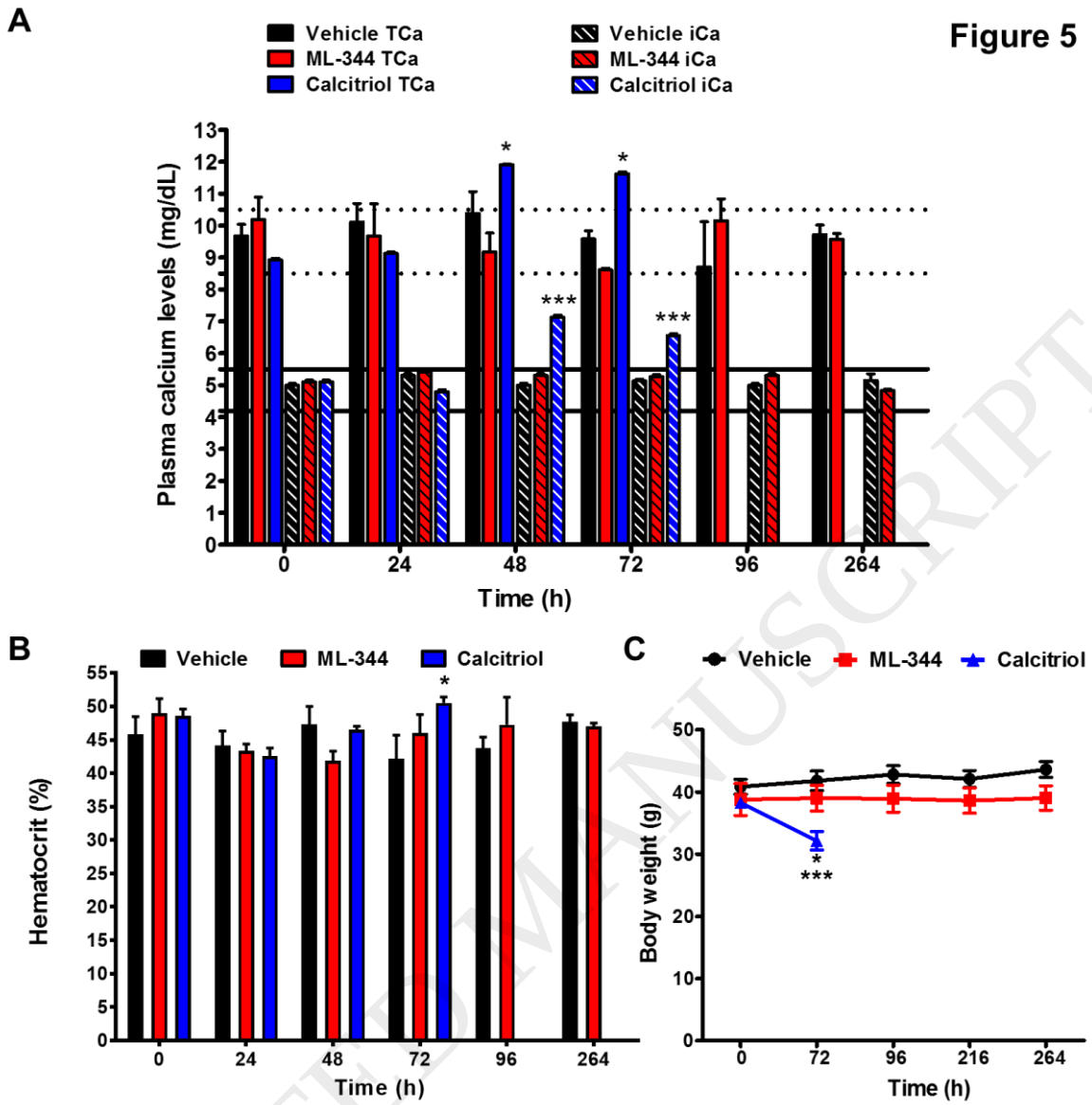

Figure 5. Effect of ML-344 analog on calcemic levels, hematocrit and animal weight of CF1 mice. A) Plasma calcium levels, **B)** hematocrit and **C)** body weight of the animals, which were injected intraperitoneally with 9 doses of 5 µg/Kg of ML-344, calcitriol or vehicle over 11 days. The graphs show the mean ± SD. Values for calcitriol beyond 72 h were not available because the animals died following 3 days of treatment. Two-way ANOVA and Bonferroni posttest were applied. TCa: total calcium. iCa: ionized calcium. Dotted lines indicate normal range of total calcium values and solid lines indicate normal range of ionized calcium levels. A: *p<0.05 and ***p<0.001 with respect to ML-344; B: *p<0.05 with respect to vehicle; C: ***p<0.001 with respect to vehicle and *p<0.05 with respect to ML-344.

3.3. COMPUTATIONAL STUDIES

Based on the interesting antitumor actions elicited by ML-344, and knowing that calcitriol exerts its antineoplastic effects through its binding to the

VDR, we decided to study at an atomistic level the binding of ML-344 to the receptor by molecular modeling techniques. The interaction patterns were compared with those of the natural hormone. Furthermore, considering that it has been vastly reported that the pH environment of tumor cells is more acidic than that of normal cells [32, 33], the pharmacodynamic features of the interaction of ML-344 and calcitriol with VDR were studied and compared at two pH values: 5.5 and 7. Figure 6 presents the binding of calcitriol and the analog ML-344 to VDR as obtained by means of molecular docking studies. As can be seen in this figure, at both pH values the binding of calcitriol to VDR is stabilized by almost the same intermolecular contacts, with several Van der Waals and hydrogen bond interactions being involved (Fig. 6 A and B). As expected in light of our previous results [34] hydrogen bond interactions between calcitriol and Tyr143, Ser237, Arg274, Ser278 and His305 were observed.

When the binding of ML-344 to VDR was analyzed at both pH values, we observed that most of the intermolecular interactions described for calcitriol are maintained (Fig. 6 C and D). Noteworthy, an additional electrostatic (EEL) contact with His397 was found, which may in turn confer differential affinity of ML-344 for VDR respect to calcitriol. As a consequence of the different ionization state of His residue at pH 5.5 and 7, in the first case the negatively charged carboxylate of ML-344 established an ionic interaction with the positively charged His397 residue, while at pH 7 an ion-dipole interaction was observed. This differential pharmacodynamic behavior may justify the selective anticancer activity of ML-344 against tumor respect to normal cells.

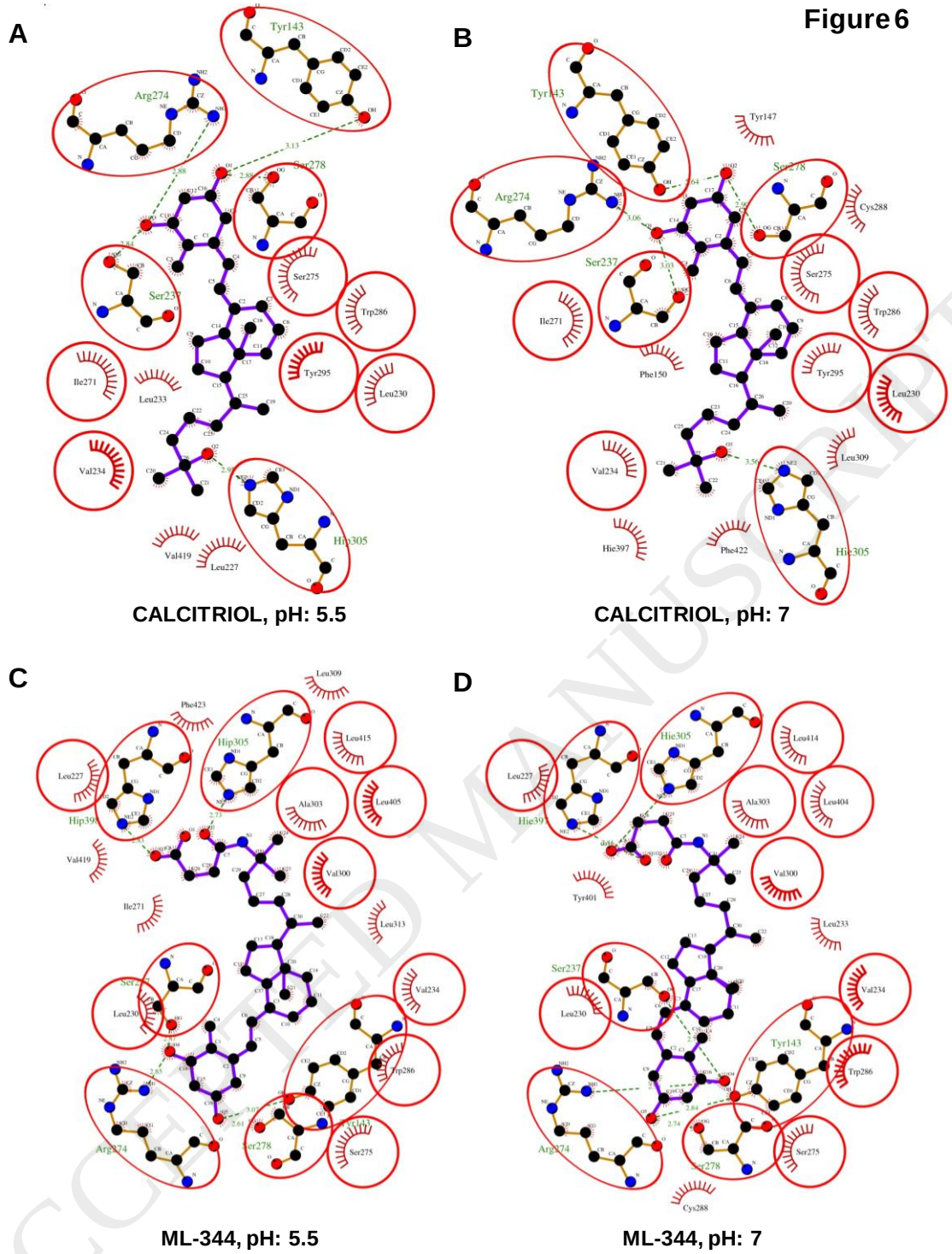

Figure 6. Molecular docking assays. Intermolecular interactions between calcitriol or ML-344 and crystal structure of the VDR at pH: 5.5 and pH: 7.

To further study this feature, molecular dynamics (MD) simulations were performed under explicit solvent conditions and physiological temperature. From the corresponding trajectories, a quantitative analysis of the interaction energies between calcitriol and ML-344 with VDR was assessed by applying the molecular mechanics Poisson-Boltzmann surface area (MM-PBSA) approach [28]. Table 2

presents the corresponding energies for each interaction component for calcitriol and ML-344 at both pH values.

Table 2. Intermolecular interaction components calculated from MD trajectories (80 ns) corresponding to the interaction of calcitriol and ML-344 with VDR.

Component	pH 5.5 (Kcal/mol)		pH 7 (Kcal/mol)	
	Calcitriol	ML-344	Calcitriol	ML-344
Van der Waals	-60.1	-69.4	-63.5	-71.6
Electrostatic	-33.2	-80.4	-27.2	9.7
Gas	-93.3	-149.8	-90.8	-61.9
Non-Polar solv.	-8.1	-9.4	-8.4	-9.7
Polar solv.	25.7	78.6	25.6	-10.9
Total	-75.8	-80.5	-73.5	-82.5

From the analysis of calcitriol component, no significant differences were observed regarding the affinity for VDR at both pH values. In agreement with our previous reports [30,34], the binding of calcitriol at both pHs is mainly stabilized by Van der Waals interactions (-60.1 and -63.5 Kcal/mol at pH 5.5 and 7, respectively), with a lesser contribution of the EEL component (-33.2 and -27.2 Kcal/mol at pH 5.5 and 7, respectively). The total interaction energies were -75.8 and -73.5 Kcal/mol, for pH 5.5 and 7, respectively, with no significant differences in the energetic components contributions, which suggests that no marked differences in the binding affinity is expected for calcitriol to VDR in tumor or normal cells. When the binding of ML-344 was analyzed, although no significant differences in the total binding affinities were found in both conditions (-80.5 and -82.5 Kcal/mol for pH 5.5 and 7, respectively), it is noteworthy that significant differences were observed in the associated interaction components, particularly the EEL one (-80.4 and 9.7 Kcal/mol for pH 5.5 and 7, respectively). In this way, a marked stabilization of the intermolecular complex is elicited by the EEL component at pH 5.5, while at pH 7 a positive energy value was calculated. To identify the amino acid residues originating this differential behavior, a per-residue interaction decomposition was performed on the corresponding MD trajectories, with the EEL components at pH 7 being subtracted from those at pH 5.5 (Fig. 7). As can be seen, at pH 7 an EEL repulsion takes place between the

negatively charged carboxylate moiety and His305 and His397 belonging to VDR. In counterpart, a strong EEL attraction is observed when these two residues are positively charged at pH 5.5. These observations suggest that ML-344 exhibits a high affinity for VDR at pH 5.5 and a lower one at pH 7. Taking into account the antineoplastic effects displayed by the analog, these observations suggest a selective antitumor activity against tumor cells respect to normal cells based on a selective binding to VDR at pH 5.5 in tumor cells. These observations derived from the molecular modeling studies are consistent with the selective antiproliferative and antimigratory properties determined for ML-344 against tumor cell lines.

Figure 7

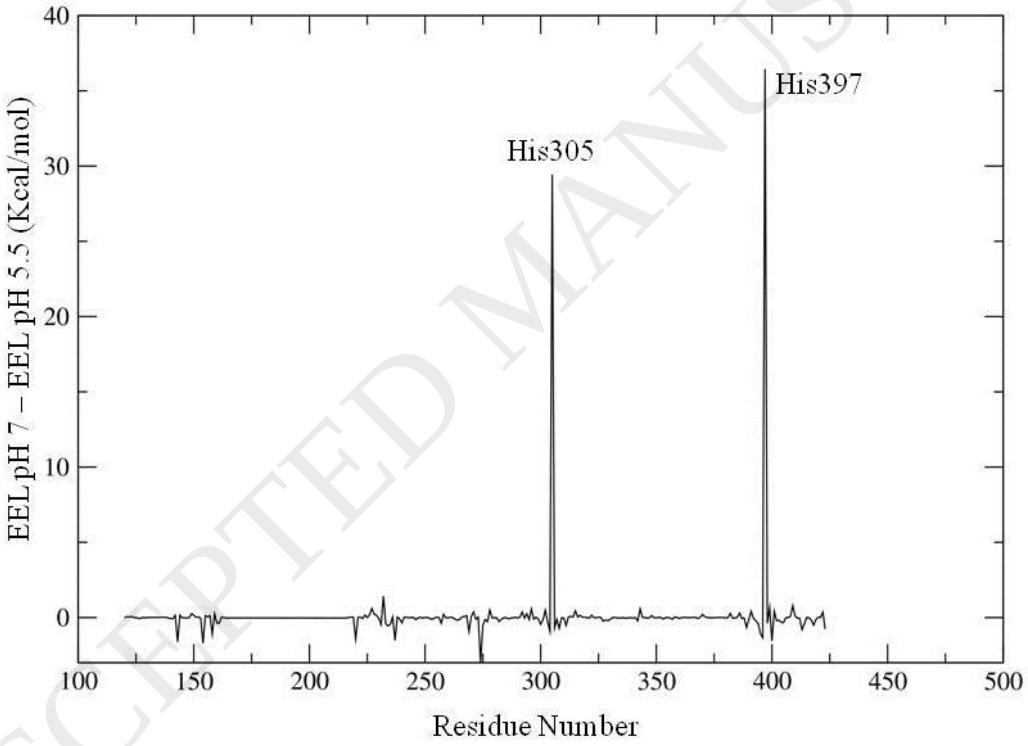

Figure 7. Difference between the EEL interaction component calculated for the interaction between ML-344 and VDR at pH 7 and that determined at pH 5.5.

4. DISCUSSION AND CONCLUSIONS

There are few previous studies of calcitriol analogs with nitrogen atoms in their chemical structure. Of these reports, a small number had examined their effects employing cell-based assays. Matsuo and col. [35] reported the synthesis

of 2α-substituted calcitriol analogs that contained nitrogen atoms in heteroaromatic ring. These compounds had shown the ability to form hydrogen bonds with Arg274 of human VDR and displayed biological effects on osteosarcoma cells. In relation to calcitriol analogs carrying nitrogen in its side chain, Takenouchi and col. [36] synthesized a series of vitamin D_3 lactone derivatives most of which displayed VDR antagonist activity whereas interestingly enough, the compound with a nitrogen atom in its side chain did not. Finally, Sinishtaj and col. [37] prepared two calcitriol analogs with amide groups in their side chain that elicited growth-inhibitory effects on murine keratinocyte cells and low-calciuric activity respect to calcitriol. In this work, we report the synthesis and biological evaluation of ML-344 that was obtained by a very efficient synthetic route based on an allylic substitution catalyzed by Pd. Moreover, ML-344 lacks the traditional terminal hydroxyl group and has an amide bonded to C-25 and a carboxyl group in its side chain. We herein demonstrate that this analog still maintains the antitumoral activities of calcitriol while it does not show hypercalcemic effects in mice. It is worth mentioning that the characteristics of the chemical structure of this compound cause that ML-344 display several particularities when binding to VDR at different pHs, which may account for the differential action between tumor and non-malignant cells. In contrast, calcitriol does not elicit these pH-dependent differences justifying its similar effects on cell viability and cell migration of both normal and tumor cells tested.

With respect to the effects of the compounds on glioblastoma cells, both ML-344 and calcitriol decreased cell viability of U251 and GL26 cell lines. Neither the analog nor calcitriol had effects on T98G cell viability. These results are in concordance with those reported by Zou and col. who reported an IC_{50} higher than 1×10^{-7} M for calcitriol in T98G cell viability assays [38]. Regarding compound effects on normal cells, the ML-344 analog did not affect the viability of human astrocytes. We suggest that the differential effect of ML-344 between glioma cells and their normal counterpart (astrocytes) may be due to its differential binding to VDR at different pHs, as demonstrated by in silico assays. Particularly for this type of cancer, reduced pH in human glioma tissues compared to the normal surrounding tissue has been demonstrated [39].

Regarding breast cancer, ML-344 has antiproliferative and antimetastatic effects on the 4T1 triple-negative and on the LM3 hormone-independent breast cancer cell lines. Triple-negative and hormone-independent breast cancers have few treatment options that present limited success. Hence, it is important to explore novel therapeutic options. In this regard, approximately two-thirds of triple-negative breast cancer tumors co-express androgen receptor and VDR or express VDR alone [42]. Therefore, the fact that ML-344 displays antitumor effects in breast cancer cells, exhibits a high affinity for VDR at acidic pH and does not provoke hypercalcemia in mice administered at continuous doses suggests its potential use as chemotherapeutic agent to treat this aggressive pathology.

In summary, all the results obtained suggest that the amide group bonded to C-25 and the carboxyl group incorporated in the side chain of ML-344 confer a higher affinity to VDR with respect to calcitriol. Furthermore, these chemical modifications may be responsible for the pH-dependent binding of the analog to VDR: at acidic pH (tumor microenvironment), greater electrostatic interactions are established than at neutral pH (normal microenvironment). These binding particularities justify the differential action between the tumor and normal cells found in the *in vitro* assays. Altogether, these properties make ML-344 a promising antitumor agent for cancer therapy.

CONFLICT OF INTEREST

The authors declare no conflicts of interest.

ACKNOWLEDGEMENTS

This work was supported by the Agencia Nacional de Promoción Científica y Tecnológica (ANPCyT, PICTs 2007-1797 and 2012-0966), Consejo Nacional de Investigaciones Científicas y Técnicas (CONICET, PIP 112-201101-00556), Universidad Nacional del Sur, Bahía Blanca, Buenos Aires, Argentina (PGI 24/B174) and by the Xunta de Galicia (ED431C2017/70). María J. Ferronato, Diego J. Obiol, Eliana N. Alonso and Silvina M. Grioli were recipients of a fellowship from CONICET. A. Martínez is grateful to the University of Vigo for predoctoral fellowship. The work of the NMR and MS divisions of the research support services of the University of Vigo (CACTI) is also gratefully

acknowledged. The authors would like to thank the CCAD – Universidad Nacional de Córdoba (http://ccad.unc.edu.ar/) and the GPGPU Computing Group from the Facultad de Matemática, Astronomía y Física (FAMAF), Universidad Nacional de Córdoba, Argentina, for providing access to computing resources. Mario A. Quevedo wishes to thank OpenEye Scientific Software and their Free Academic Licensing for providing licenses to use the corresponding software packages. Finally, Mario A. Quevedo thanks the NVIDIA GPU Grant Program program, for providing GPU infrastructure.

REFERENCES

[1] Bandera Merchan, B., Morcillo, S., Martin-Nuñez, G., Tinahones, J.F., & Macías-González, M. (2017). The role of vitamin D and VDR in carcinogenesis: Through epidemiology and basic sciences. *Journal of Steroid Biochemistry and Molecular Biology*, *167*, 203-218. doi: 10.1016/j.jsbmb.2016.11.020.

[2] Christakos, S., Dhawan, P., Verstuyf, A., Verlinden, L., & Carmeliet, G. (2016). Vitamin D: metabolism , molecular mechanism of action , and pleiotropic effects vitamin d analogs. *Physiological Reviews*, *3*, 365- 408. doi: 10.1152/physrev.00014.2015.

[3] Duffy, M. J., Murray, A., Synnott, N. C., Donovan, N. O., & Crown, J. (2017). Vitamin D analogues: Potential use in cancer treatment. *Critical Reviews in Oncology / Hematology*, *112*, 190-197. doi: 10.1016/j.critrevonc.2017.02.015.

[4] Deeb, K. K., Trump, D. L., & Johnson, C. S. (2007). Vitamin D signaling pathways in cancer : potential for anticancer therapeutics. *Nature Reviews Cancer, 7* (9), 684-700.doi: 10.1038/nrc2196.

[5] Vuolo, L., Somma, C. D., Faggiano, A., & Colao, A. (2012). Vitamin D and cancer. *Frontiers in Endocrinology*, *3*, 1-13. doi: 10.3389/fendo.2012.00058.

[6] Wang, Y., Zhu, J., & DeLuca, H. F. (2012). Where is the vitamin D receptor? *Archives of Biochemistry and Biophysics*, *523*(1), 123–133. doi: 0.1016/j.abb.2012.04.001

[7] Rai, V., Abdo, J. O. E., Agrawal, S., & Agrawal, D. K. (2017). Vitamin D Receptor Polymorphism and Cancer: An Update. *Anticancer Research*, *37*(8), 3991–4003. doi: 10.21873/anticanres.11784

[8] Campbell, M. J. (2014). Vitamin D and the RNA transcriptome: more than mRNA regulation. *Cancer*, *5*, 1-13. doi: 10.3389/fphys.2014.00181.

[9] Ferronato, M. J., Salomón, D. G., Fermento, M. E., Gandini, N. A., López Romero, A., Rivadulla, M. L., et al. (2015). Vitamin D Analogue: Potent Antiproliferative Effects on Cancer Cell Lines and Lack of Hypercalcemic Activity. *Archiv der Pharmazie*, *348*(5), 315-329. doi: 10.1002/ardp.201400448.

[10] Ferronato M.J., Obiol D.J., Fermento M.E., Gandini N.A., Alonso E.N., Salomón D.G. et al. (2015) The alkynylphosphonate analogue of calcitriol EM1 has potent anti-metastatic effects in breast cancer. *The Journal of steroid*

biochemistry and molecular biology, *154*,285-93, doi: 10.1016/j.jsbmb.2015.09.009.

[11] Salomón, D. G., Grioli, S. M., Buschiazzo, M., Mascar, E., Vitale, C., Radivoy, G., et al. (2011). Novel Alkynylphosphonate Analogue of Calcitriol with Potent Antiproliferative Effects in Cancer Cells and Lack of Calcemic Activity. *ACS Medicinal Chemistry Letters. 2*(7),503-508*.* doi: 10.1021/ml200034w.

[12] Rochel, N., Wurtz, J. M., Mitschler, A., Klaholz, B., & Moras, D. (2000). The crystal structure of the nuclear receptor for vitamin D bound to its natural ligand. *Molecular cell*, *5*(1), 173-179. doi: 10.1016/S1097-2765(00)80413-X.

[13] Maier, J. A., Martinez, C., Kasavajhala, K., Wickstrom, L., Hauser, K. E., & Simmerling, C. (2015). ff14SB: improving the accuracy of protein side chain and backbone parameters from ff99SB. *Journal of chemical theory and computation*, *11*(8), 3696-3713. DOI 10.1021/acs.jctc.5b00255.

[14] MarvinSketch v.6.31, ChemAxon Ltd., http://www.chemaxon.com.

[15] Frisch, M.J., Trucks, G.W., Schlegel, H.B., Scuseria, G.E., Robb, M.A., Cheeseman,J.R., et al. (2016). Gaussian 09, Gaussian, Inc.

[16] Wang, J., Wolf, R. M., Caldwell, J. W., Kollman, P. A., & Case, D. A. (2004). Development and testing of a general amber force field. *Journal of computational chemistry*, *25*(9), 1157-1174. DOI: 10.1002/jcc.20035.

[17] Jakalian, A., Bush, B. L., Jack, D. B., & Bayly, C. I. (2000). Fast, Efficient Generation of High-Quality Atomic Charges. AM1-BCC Model: I. Method. *Journal of Computational Chemistry*, *21*(2), 132–146. doi: 10.1002/(SICI)1096-987X(20000130)21:2<132::AID-JCC5>3.0.CO;2-P

[18] OpenEye. Scientific.Software, Santa Fe, NM, http://www.eyesopen.com.

[19] Omega.2.4.3. OpenEye Scientific Software, Santa Fe, NM http://www.eyesopen.com.

[20] Hawkins, P. C., Skillman, A. G., Warren, G. L., Ellingson, B. A., & Stahl, M. T. (2010). Conformer generation with OMEGA: algorithm and validation using high quality structures from the Protein Databank and Cambridge Structural Database. *Journal of chemical information and modeling*, *50*(4), 572-584. doi: 10.1021/ci100031x.

[21] Fred.3.0.0 OpenEye.Scientific.Software, Santa Fe, NM, http://www.eyesopen.com.

[22] McGann, M. (2012). FRED and HYBRID docking performance on standardized datasets. *Journal of computer-aided molecular design*, *26*(8), 897-906. doi: 10.1007/s10822-012-9584-8.

[23] VIDA.4.2.1. OpenEye Scientific Software, Santa Fe, NM http://www.eyesopen.com.

[24] Laskowski, R. A., & Swindells, M. B. (2011). LigPlot+: multiple ligand–protein interaction diagrams for drug discovery. J. Chem. Inf. Model*, 51* (10), 2778–2786. doi: 10.1021/ci200227u.

[25] Case, D. A., Cheatham, T. E., Darden, T., Gohlke, H., Luo, R., Merz, K. M., et al. (2005). The Amber biomolecular simulation programs. *Journal of computational chemistry*, *26*(16), 1668-1688. doi: 10.1002/jcc.20290.

[26] Salomon-Ferrer, R., Case, D. A., & Walker, R. C. (2013). An overview of the Amber biomolecular simulation package. *Wiley Interdisciplinary Reviews: Computational Molecular Science*, *3*(2), 198-210. DOI 10.1002/wcms.1121.

[27] Kuhn, B., Gerber, P., Schulz-Gasch, T., & Stahl, M. (2005). Validation and use of the MM-PBSA approach for drug discovery. *Journal of medicinal chemistry*, *48*(12), 4040-4048. doi: 10.1021/jm049081q.

[28] Miller Iii, B. R., McGee, T. D., Swails, J. M., Homeyer, N., Gohlke, H., & Roitberg, A. E. (2012). MMPBSA.py: An efficient program for end-state free energy calculations. *Journal of Chemical Theory and Computation, 8*(9), 3314-3321, doi: 10.1021/ct300418h.

[29] Rivadulla, M. L., Pérez-garcía, X., Pérez, M., Gómez, G., & Fall, Y. (2013). Pd-allylic substitution mediated synthesis of 25-amino vitamin D 3 derivatives. *Tetrahedron Letters*, *54*(24), 3164-3166. doi: 10.1016/j.tetlet.2013.04.019.

[30] Ferronato, M.J., Alonso, E.N., Salomón, D.G., Fermento, M,E., Gandini, N.A., Quevedo, M.A., et al. (2018). Antitumoral effects of the alkynylphosphonate analogue of calcitriol EM1 on glioblastoma multiforme cells. *The Journal of steroid biochemistry and molecular biology, 178,* 22-35. doi: 10.1016/j.jsbmb.2017.10.019.

[31] Katayama, M. L. H., Pasini, F. S., Folgueira, M. A. A. K., Snitcovsky, I. M. L., & Brentani, M. M. (2003). Molecular targets of 1, 25 (OH) $_2$ D $_3$ in HC11 normal mouse mammary cell line. *The Journal of steroid biochemistry and molecular biology*, *84*(1), 57-69. doi: 10.1016/S0960-0760(03)00004-9.

[32] Gerweck L.E., Seetharaman K. (1993). Cellular pH gradient in tumor versus normal tissue: potential exploitation for the treatment of cancer. *Cancer Research*, 56(6),1194-1198.

[33] Hruby, M., & Ulbrich, K. (2005). Polymeric micellar pH-sensitive drug delivery system for doxorubicin. *Journal of Controlled Release*, *103*, 137-148. doi: 10.1016/j.jconrel.2004.11.017.

[34] Ferronato, M. J., Alonso, E. N., Gandini, N. A., Fermento, M. E., Villegas, M. E., Quevedo, M. A., et al. (2016). The UVB1 Vitamin D analogue inhibits colorectal carcinoma progression. *The Journal of steroid biochemistry and molecular biology*, *163*, 193-205. doi: 10.1016/j.jsbmb.2016.05.019.

[35] Matsuo, M., Hasegawa, A., Takano, M., Saito, H., Kakuda, S., Chida, T., et al. (2013). Synthesis of 2α-Heteroarylalkyl Active Vitamin D 3 with Therapeutic Effect on Enhancing Bone Mineral Density in Vivo. *ACS Medicinal Chemistry Letters*, 4 (7), 671-674. doi: 10.1021/ml400098w.

[36] Takenouchi, K., Sogawa, R., Manabe, K., Saitoh, H., Gao, Q., Miura, D., et al. (2004). Synthesis and structure – activity relationships of TEI-9647 derivatives as Vitamin D3 antagonists. *Journal of Steroid Biochemistry*, *90*, 31-34. doi: 10.1016/j.jsbmb.2004.03.046.

[37] Sinishtaj, S., Jeon, B., Dolan, P., Kensler, T. W., & Posner, G. H. (2006). hydroxamate analogs of the hormone 1a , 25-dihydroxyvitamin D 3. *Bioorganic & Medicinal Chemistry*, *14*, 6341-6348. doi: 10.1016/j.bmc.2006.05.050.

[38] Zou, J., Landy, H., Feun, L., Xu, R., Lampidis, T., Wu, C. J., et al. (2000). Correlation of a Unique 220-kDa Protein with Vitamin D Sensitivity in Glioma Cells. *Science*, *60*(00), 1361-1365. doi: 10.1016/S0006-2952(00)00438-X.

[39] Hjelmeland, A.B., Wu, Q., Heddleston, J.M., Choudhary, G.S., MacSwords J., Lathia, J.D., McLendon R., Lindner, D., Sloan, A., Rich J.N. (2011). Acidic stress promotes a glioma stem cell phenotype. *Cell Death Differentiation*, *18(5),* 829–840. doi: 10.1038/cdd.2010.150

[40] Senkus, E., Kyriakides, S., Ohno, S., Penault-Llorca, F., Poortmans, P., Rutgers, E., et al. (2015). Primary breast cancer: ESMO Clinical Practice Guidelines for diagnosis, treatment and follow-up. *Annals of Oncology, 26*, 8–30. doi: 10.1093/annonc/mdv298.

[41] Collignon, J., Lousberg, L., Schroeder, H., & Jerusalem, G. (2016). Triple-negative breast cancer: treatment challenges and solutions. *Breast Cancer : Targets and Therapy*, *8*, 93-107. doi: 10.2147/BCTT.S69488.

[42] Thakkar, A., Buchwald, B. W. M. P.-ruiz P., & Ince, T. A. (2016). Vitamin D and androgen receptor-targeted therapy for triple-negative breast cancer. *Breast Cancer Research and Treatment*, *157*(1), 77-90. doi: 10.1007/s10549-016-3807-y.

Table 1. IC_{50} of cells that responded to ML-344 or calcitriol treatment (nM).[a]

Cells	ML-344	Calcitriol	Cells	ML-344	Calcitriol
LM3	1.007	-	GL26	0.016	0.118
4T1	7.650	0.618	U251	0.457	0.043
HC11	-	0.599	T98G	-	-
HN13	-	3.337	Astrocytes	-	30.80
HN12	3.679	2.335			

[*a*] IC_{50}: Half maximal inhibitory concentration (nM)

Table 2. Analysis of cellular DNA content by flow cytometry

	Vehicle (%)	**ML-344 (%)**
Sub G0/G1	13.02 ± 0.29	14.83 ± 1.36
G0/G1	53.53 ± 2.07	60.74 ± 2.04
S	24.23 ± 0.98	16.94 ± 1.55
G2/M	9.21 ± 0.67	7.49 ± 0.65

Table 3. Intermolecular interaction components calculated from MD trajectories (80 ns) corresponding to the interaction of calcitriol and ML-344 with VDR.

Component	pH 5.5 (Kcal/mol)		pH 7.0 (Kcal/mol)	
	Calcitriol	**ML-344**	**Calcitriol**	**ML-344**
Van der Waals	-60.1	-69.4	-63.5	-71.6
Electrostatic	-33.2	-80.4	-27.2	9.7
Gas	-93.3	-149.8	-90.8	-61.9
Non-Polar solv.	-8.1	-9.4	-8.4	-9.7
Polar solv.	25.7	78.6	25.6	-10.9
Total	-75.8	-80.5	-73.5	-82.5